

RESEARCH ARTICLE

Ambient Air Monitoring System With Adaptive Performance Stability

RADY PURBAKAWACA¹, (Graduate Student Member, IEEE), ARIEF SABDO YUWONO²,
I. DEWA MADE SUBRATA¹, SUPANDI³, AND HUSIN ALATAS^{4,5}

¹Department of Mechanical and Biosystems Engineering, IPB University, Bogor 16680, Indonesia

²Department of Civil and Environmental Engineering, IPB University, Bogor 16680, Indonesia

³Unilab Perdana, Jakarta 12230, Indonesia

⁴Department of Physics, IPB University, Bogor 16680, Indonesia

⁵Center for Transdisciplinary & Sustainability Sciences (CTSS), IPB University, Bogor 16128, Indonesia

Corresponding author: Husin Alatas (alatas@apps.ipb.ac.id)


This work was supported by the Unilab Perdana Laboratory through Bogor Agricultural University (IPB) University. The work of Husin Alatas was supported by World Class Research (WCR) Grant 2022 from the Ministry of Education, Culture, Research, and Technology, Republic of Indonesia, under contract no. 3732/IT3. L1/PT.01.03/P/B/2022.

ABSTRACT Air pollution is a significant concern in this era. However, large quantities of pollutants can cause environmental damage and human health problems. The existing monitoring systems are highly precise and sensitive; however, they require high laboratory analysis and high operational costs. To overcome these problems, an air quality monitoring system has been proposed as an alternative that can complement the current system. This study aimed to design an inexpensive air quality monitoring system using metal oxide sensors to measure the concentrations of carbon monoxide (CO), nitrogen dioxide (NO₂), sulfur dioxide (SO₂), and particulate matter (PM) using laser diffraction, a microcontroller, and a general packet radio service module. Our air quality index monitoring system is a sensor node powered by a rechargeable battery supplied by either a solar panel or an alternating current power supply. Our developed system is equipped with an information system, namely a server and graphical user interface, to receive data, calculate the air pollutant standard index, and access data. In this paper, we discussed a novel adaptive algorithm for reducing packet loss in cellular-network-based transmissions. This algorithm allows nodes to perform repeated data transmissions and extends the response waiting times according to the received signal strength indicator. The test results show that the developed algorithm can reduce packet loss by 9.8–11.6% under medium/bad conditions. The node test was carried out in a heavy traffic area approximately 2 km from Atang Senjaya Airport with moderate air quality.

INDEX TERMS Adaptive algorithm, air pollution monitoring, air quality monitoring, low-cost sensors.

I. INTRODUCTION

Many studies on the adverse effects of air pollution exposure on human health and the environment have been scientifically confirmed in recent decades [1], [2], [3]. In the agricultural sector, air pollution affects crop yields and can have adverse social and economic effects in developing countries [4]. Therefore, air pollution is an urgent problem in the United Nations Sustainable Development Goals (SDGs).

The associate editor coordinating the review of this manuscript and approving it for publication was Liang-Bi Chen .

Targets substantially reduce the health impacts of hazardous substances and human health [5].

Air pollution monitoring is essential to increase public awareness of sustainable urban environments and human health. Unfortunately, the equipment required to meet the regulatory standards for air quality monitoring has high procurement and maintenance costs, despite the high accuracy and selectivity of the measured parameters. In Indonesia, air quality monitoring systems are based on government regulations, which are limited to the measurement of the air pollutant quality standard index (ISPU), namely nitrogen dioxide (NO₂), sulfur dioxide (SO₂), carbon

monoxide (CO), ozone (O₃), hydrocarbons (HC), and particulate matter (PM_{2.5}, PM₁₀) [6].

One possible solution to complement conventional methods is to design a low-cost air pollutant monitoring device that can transmit air pollutant data in real time. Many innovative methods have been proposed that use low-cost sensors integrated with various data-transmission devices. For example, the application of metal oxide sensors (MOX), electrochemical gas sensors, and particulate matter sensors integrated with wireless network technology can increase the coverage area and spatial resolution of monitoring systems reported in the literature [7]. The standard communication protocols used in wireless network technologies include cellular, Zigbee, Lora, and Wi-Fi, among others, which can be used as air quality measuring instruments and support widespread device placement in remote areas. The advantage of this approach is that air quality monitoring systems can display air pollutant concentrations in real-time.

Air quality monitoring using wireless sensor networks has been widely reported in the literature. Bagula et al. [8] presented an air quality monitoring system with an integrated ubiquitous sensor network for development (USN4D) architecture for opportunistic data dissemination, remote deployment, and information localization using General Packet Radio Service (GPRS) and XbeePro cellular networks with multi-star topologies. USN4D reported that the GPRS and Zigbee packet losses reached 10%. Rahmat et al. [9], [10], [11] succeeded in designing sensors based on crystal photonics and an air quality monitoring system based on numerical analysis of one-dimensional photonic crystals developed by Alatas et al. [12]. The developed system could detect NO₂ and O₃ pollutant levels under ambient conditions and send data via the XBee protocol wireless sensor network.

Azis et al. [9] demonstrated a low-cost air quality monitoring system using gas sensors, nitrogen dioxide, carbon monoxide, sulfur dioxide, particulate sensors, and surface ozone. This system can calculate the air quality index and determine the air quality status in real time and near real time through desktop and web applications via Xbee protocol communication. Developing a Hybrid Tree-Like Mesh network topology proposed by Iqbal et al. [13] using Zigbee and GPRS for air quality monitoring systems has increased data throughput by 32.06%, reducing delay by 23.28%, and packet loss ratio by 0.01%. A Global System for Mobile Communications modem-based cellular monitoring system was developed and tested in Sharjah, UAE, by Al-Ali et al. [14] The system consists of two main parts: mobile data acquisition and a monitoring server (pollution-server). The measurement data were transmitted via a cellular network using a GPRS modem to the pollution server. However, this approach does not appear to be suitable for large-scale deployments. They did not calibrate the sensors and reported the quality of the service for data transmission.

One of the most important aspects of air quality monitoring systems is reliability of data transmission which depends

on the quality of the related wireless communication platform. The most developed low-cost air quality monitoring system transmits data using wireless communication based on cellular, Zigbee, and Lora communication [15], [16], [17]. A study by [18] showed that dynamic weather results in a significant decrease in the accuracy of distance estimation based on the received signal strength of a Global System for Mobile Communications (GSM). In the meantime, the results of a study conducted by [19], [20] showed that a decrease in the packet-receive ratio (PRR) often decreases the received signal strength indicator (RSSI) owing to an increase in the distance between the receiver and transmitter and a decrease in the transmit power level. However, wireless communications used in air quality monitoring systems are susceptible to environmental dynamics, which can hinder data transmission performance. The reliability of data transmission can affect the temporal resolution of the air quality monitoring data. This underlies research on developing an adaptive algorithm based on RSSI to set the response waiting time based on the received signal strength of the GSM/GPRS signals. This study also examined the effect of changes in the response time variations on the packet loss ratio and latency of the SIM7000E modem as a transmitter in a static air quality monitoring system.

Opportunities to use low-cost air quality sensors to benefit individuals and national communities are open. This inexpensive device is not intended to replace existing air quality monitoring stations but helps increase the spatial range of complimentary air pollution measurements [8], [13], [14], [15], [17], [21], [22], [23]. However, several factors are related to the technical challenges of developing and implementing low-cost air quality sensors to produce quality data, evaluate sensors, and integrate sensors obtained from various sources need to be considered [24]. High spatiotemporal air quality monitoring systems require a network that can provide broad coverage and high data transmission rates with minimal data loss.

This paper proposes an air quality monitoring system based on GPRS wireless technology. An air quality monitoring system prototype was proposed based on the following electronic components: a microcontroller, GSM/GPRS module, sulfur dioxide (SO₂) sensor, carbon monoxide (CO) sensor, nitrogen dioxide (NO₂) sensor, particulate matter (PM) sensor, and weather sensors (air temperature, air pressure, relative humidity, wind speed, rainfall, and direction). The contribution of this study mainly emphasizes the role of the GPRS module as a real-time data-transfer component. This study also builds an adaptive algorithm for data transmission through cellular networks based on variations in the received signal strength of the GSM/GPRS signals. These results over relatively stable cellular data transmission systems increase the possibility of data transmission and minimize packet loss compared to devices without adaptive algorithms. The proposed air quality monitoring system is deployed and operated in an urban environment.

II. PROPOSED APPROACH

This research was conducted comprehensively through modeling and simulation, experimentation and instrumentation, and the application of information technology. First, modeling and simulation were performed to describe the physical phenomena of the chamber and the gas sampling. Experiments and instrumentation were conducted to test the sensor performance and to transmit data. Finally, information technology is applied to collect, display, and process the data. Figure 1 illustrates the flow of this study.

The system designed in this study used low-cost and readily available components (common parts). Consequently, the production costs are affordable and facilitate further system development. The developed system consists of a sensor node called an air quality index monitoring system (AQIMoS) and a website application. The AQIMoS device consists of three main parts: a microcontroller, sensors, and a GSM/GPRS modem that is fully integrated with solar power. The main capabilities of AQIMoS include continuously measuring pollutant levels in real time and adapting data transmission according to signal conditions.

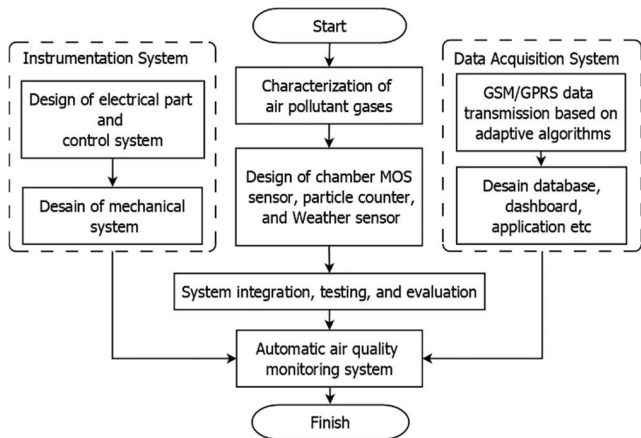


FIGURE 1. Research flow chart.

An AQIMoS instrumentation system was successfully developed by using the concept of modularity. For optimization, the AQIMoS system is divided into modules that can work independently, integrated, and controlled by the primary control system. Several AQIMoS subsystems, such as the gas sensor module, particulate sensor module, and weather sensor module, can operate properly, as shown in Figure 2.

A. MICROCONTROLLER

The MEGA+WI-FI integration board produced by Robot-Dyn was used in this study. This module combines Mega 2560 and ESP8266 microcontrollers (MCU) in a single circuit board, can be connected via universal asynchronous receiver-transmitter (UART) communication, and can run tasks in parallel. Mega 2560 (Atmel) is an 8-bit microcontroller with a 256-Kb programmable flash memory, 16 analog inputs, 54 digital I/O pins, and a clock speed of 16 MHz.

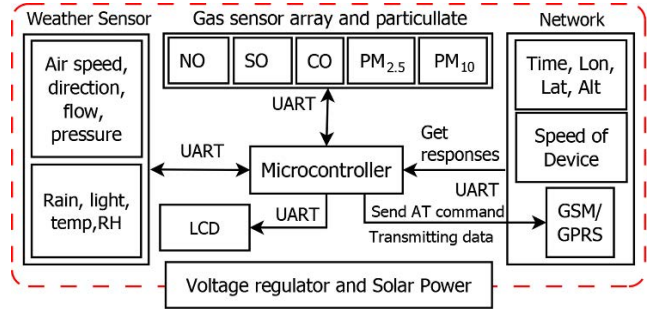


FIGURE 2. AQIMoS functional diagram.

In contrast, ESP8266 is a 32-bit microcontroller equipped with Wi-Fi 802.11 b/g/n 2.4 GHz.

The MCU plays a primary role as a control, data collection, and data-processing unit. The MCU uses UART to obtain data from gas sensors, weather, and particulate data and sends commands to SIM7000E using AT commands. The number of hardware modules integrated with the primary MCU increases complexity. This affects the identification, finding, and correction of errors in the created and tested programs. LCD actuators are required to display results or indicators that are separate from the computer.

The Nextion LCD NX4024T032 series has a clock speed of 48 MHz, 4 MB flash memory, and 3584 bytes of RAM to store variables, characters, and images. NX4024T032 is controlled using human-machine interface (HMI) technology and can run programs without relying on the capabilities of the primary MCU. The LCD communicates via the serial TTL port with the primary controller and vice versa.

B. SENSOR SPECIFICATIONS

The gas sensors used in this study were metal oxide (MOX) sensors such as MiCS-6814 (Sensortech), MQ-7 (Zhengzhou Winsen Electronics Technology), and MQ-136 (Hanwei Electronics) sensors. MOX sensors have advantages over other sensors, particularly in terms of the response time, price, and integration with instrumentation systems [25]. For particulate measurements, we used an SDS011 sensor based on light scattering. SDS011 was chosen because it can simultaneously measure particulates with diameters less than 2.5 μm (PM_{2.5}) and less than 10 μm (PM₁₀) (Table 1).

The MiCS-6814 sensor has been extensively developed to design an air quality system as an ambient NO₂ and CO sensor, with the advantages of compact design and small dimensions, robust MEMS sensors for harsh environments, and high-volume manufacturing for low-cost applications [26], [33], [34], [35]. The measured resistance value (R_s) was normalized to the air resistance (R_o) and then converted to a concentration value using the graph in the MiCS-6814 datasheet to obtain the detected pollutant concentration. The actual value of R_o depends on the environmental conditions, particularly air temperature and relative humidity.

TABLE 1. GAS and particulate sensor.

Sensor	Parameter	Specification
MiCS-6814 [26]	NO ₂	NO ₂ range, 0.5–10 ppm Voltage range, 4.9–5.1 V Relative humidity range, 5–95% Temperature range, -30–85°C
MQ-7 [27]	CO	CO range, 10–5000 ppm Voltage range, 5.0–5.1 V Relative humidity range, 5–95% Temperature range, -40–70°C
MQ-136 [28]	SO ₂	SO ₂ range, 1–100 ppm Voltage range, 5.0–5.1 V Relative humidity range, 5–95% Temperature range, -10–45°C
SDS011 [29]–[32]	PM _{2.5} PM ₁₀	Measuring range, 0–999 µg/m ³ Voltage range, 4.9–5.0 V Relative humidity range, 0–90% Temperature range, -10–50°C

TABLE 2. Weather sensor specifications.

Sensor	Parameter	Specification
Si7021 [44]	Ambient temperature and relative humidity	RH range, 0–100% Temperature range, -10–85°C Voltage range, 1.9–3.6 V Maximum current, 150 µA
MPL-3115A2 [45]	Air pressure	Pressure range, 20–110 kPa Voltage range, 1.6–3.6 V Maximum current, 40 µA
Anemometer [46]	Wind speed	A wind speed of 1.492 MPH switch to close once per second
Wind vane [46]	Wind direction	22.5 resolution of degrees of wind direction
Rain gauge [46]	Rain	A self-emptying bucket 0.2794 mm of rain

The MQ-136 sensor measured the ambient SO₂ levels in previous studies [36], [37], [38]. The results of the MQ-136 test show that the sensor can measure ambient SO₂ levels at 1-min intervals [36]. In contrast, [38] shows the MQ-136 ability to operate continuously for more than one month with hourly measurement intervals.

The light-scattering-based PM sensor that performs well under real conditions is SD011. This sensor had a fast response time and low power consumption. Evaluation studies of the SDS011 particulate sensor using standard equipment have been conducted for nearly four months [39]. The experimental results show that the SDS011 sensor has an accuracy of 80.76–98.16% compared with the reference.

The stability and nonlinearity of measuring air pollutant levels are related to ambient air conditions, weather, emissions, and other factors reported in the literature [40], [41], [42], [43]. Therefore, the Sensor Assembly p/n 80422 can be integrated with the Weather Shield (SparkFun) using an MCU to become a standalone system (Table 2). This system can collect and process meteorological data independently and transmit the data to the primary MCU via the UART.

C. MECHANICAL DESIGN

Figure 3 shows that air enters the chamber cavity and flows through the gas sensor during the sensing process. Air was sucked at a specific flow rate using a fan attached to the chamber to measure pollutants. In this study, the total volume of closed air in the section was 456.22 cm³, and it took 3.8 s to be refilled using a fan with a flow rate of 7 l/m. The flow rate was maintained using a PC817X optocoupler control circuit and IRF540 MOSFET with the PWM method, which can maintain a stable suction airflow path at the desired level [47].

D. NETWORK CONFIGURATION

Several wireless communication alternatives, such as Wi-Fi, Bluetooth, and GSM/GPRS, which can be used as data transmission protocols for air quality systems, have been reported in the literature [8], [13], [14], [15], [17], [21], [48], [49], [50], [51], [52], [53]. The GSM was chosen for this study because it allows digital communication in urban and rural areas with broad coverage. The 1800/1900 MHz band was used as a short-distance high band in urban areas, and the 850/900 MHz long-range band was used in rural areas. GPRS is a GSM for broadband cellular transactions and connects to the internet.

The SIM7000E (SIMCom Wireless Solutions Co.) is a modern GSM/GPRS variant. SIM7000E is a tri-band LTE-FDD and dual-band GPRS/EDGE wireless module that supports LTE CAT-M1 (eMTC) and NB-IoT. SIM7000E was designed for low-latency applications suitable for machine-to-machine (M2M) applications such as measurement, telematics, asset tracking, and remote monitoring [54]. Data delivery in AQIMoS refers to the basic IoT model, which consists of sensor, network, and application layers. Figure 4 shows the stages of data collection and processing using the AQIMoS at the sensor layer. The network layer receives the data sent by the device via GPRS. Finally, the application manages the data in the last layer and reaches the end-user.

E. SOFTWARE ARCHITECTURE

Communication between the primary microcontroller and other hardware modules is an essential requirement for AQIMoS devices to operate as ordered. Therefore, the Arduino program code for AQIMoS was built based on a block algorithm, according to the specific function of each module. The code consists of several main stages: configuration, network initialization, GPS data and timing capture, sensor data, JavaScript object notation (JSON) data format, and packet transmission via GSM/GPRS.

First, the configuration stores and changes variables such as the device ID, data transmission interval, and access points accessed by smartphones via Wi-Fi ESP8266 (Figure 5). The stored variables were used to adjust the operation of the Mega 2560 to match the specified configuration. The configuration was built using the Serial Peripheral Interface Flash File

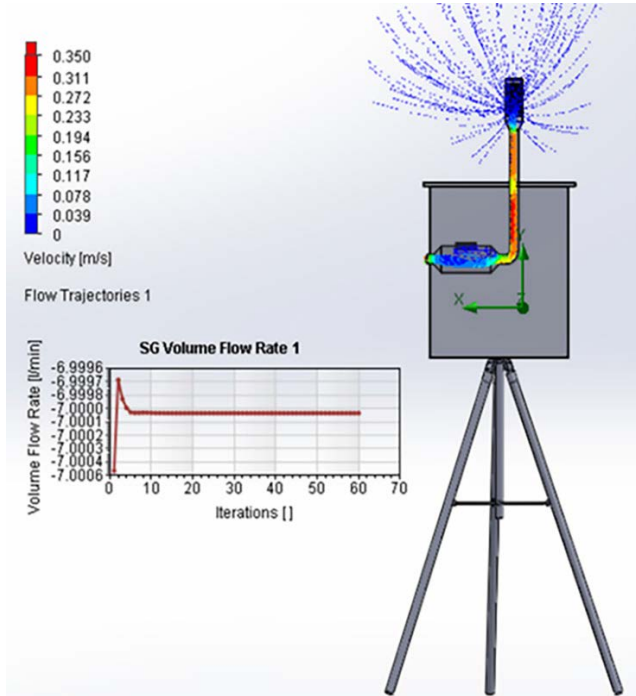


FIGURE 3. Airflow simulation of the AQIMoS chamber.

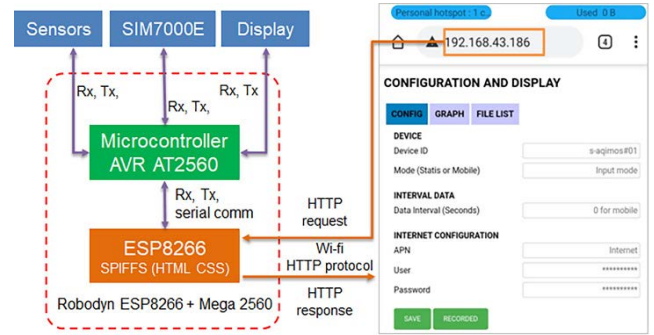


FIGURE 5. The AQIMoS configuration page over web server ESP8262 accessed via mobile browsers.

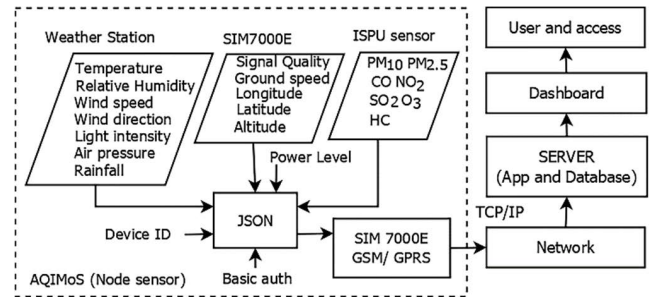


FIGURE 6. The JSON structure of the AQIMoS device.

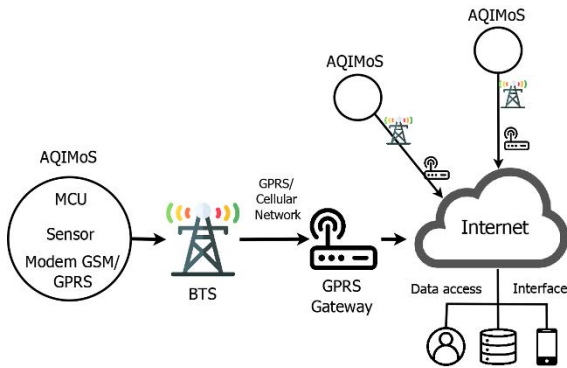


FIGURE 4. AQIMoS network.

System method by storing the HTML and CSS files in ESP8266 extra flash memory. Second, the initialized network contained a command to connect AQIMoS to the GSM/GPRS network. Third, the extracted timestamps and GPS data were retrieved in National Marine Electronics Association (NMEA) format. Fourth, all sensors were read and compiled into the JSON format. Finally, the data are sent via the Transmission Control Protocol/Internet protocol (TCP/IP), waiting for a response from the provider and central server, and evaluating the data transmission (Figure 6).

AQIMoS can send data such as time, device location, and pollution level via GSM/GPRS to a particular application server or database via the TCP/IP protocol in JSON, as shown in Figure 7. For all the gas parameters, the keys are still provided with a default value of zero. However, this study was limited to ISPU parameter measurements of NO₂, SO₂,

TABLE 3. AQIMoS JSON structure.

JSON structure (Key value)	Description
{“sTime”: “0000-00-00 00:00:00,”	– Timestamp
“Pm10”:0, “Pm25”:0, “NO2”:0,	– Pollutant concentration appropriate to the unit
“CO”:0, “SO2”:0, “O3”:0,	– Weather sensor value appropriate to the unit
“T”:0, “RH”:0, “sW”:0,	
“dW”:0, “R”:0, “P”:0, “L”:0,	
“BP”:0.0,	– Battery level in Volt
“lat”: 00.000000, “lon”:000.00000,	– Latitude, longitude, altitude, and ground speed
“alt”: 000.0, “sp”:000.0,	
“qs”:000.0,	– Signal quality level
“devID”: “device_name,”	– Unique device identity
“username”: “username”	– Basic authentication
“password”: “password”}	– Basic authentication

CO, PM_{2.5} and PM₁₀. This was intended to accommodate the addition of the gas parameters measured in further work. Table 3 presents details of the JSON structure. The measurement result data stored in the database can be accessed by users using a front-end application.

The time required for one cycle of data transmission depends on the time it takes for a sensor to read and send a packet. For example, AQIMoS transmits data continuously without fixed intervals. Weather, PM, and gas readings were performed for 1 s each time. Therefore, the weather sensor required three readings, whereas the PM and gas sensors required 100 readings. The readings were then averaged to

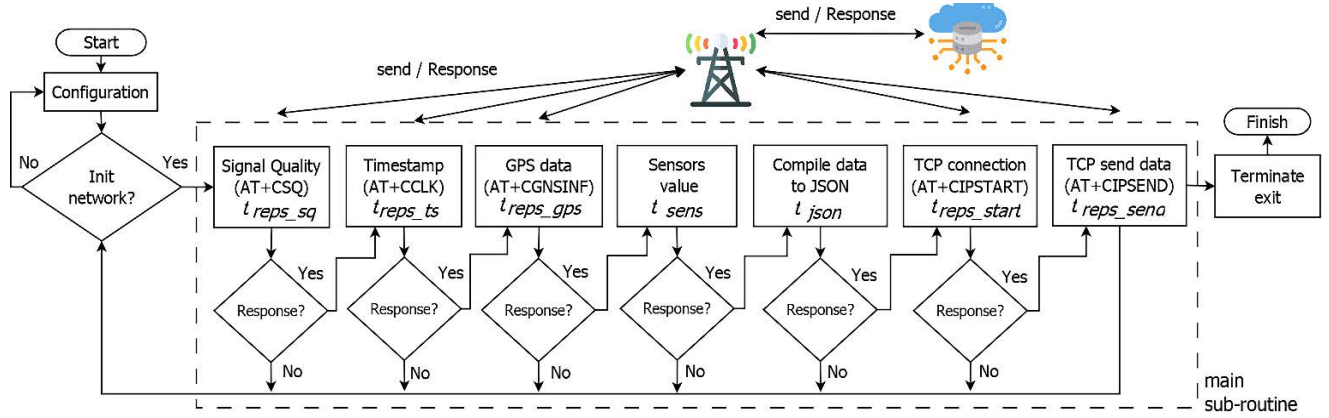


FIGURE 7. AQIMoS working system algorithm.

reduce the noise. Once collected, data were sent over the GSM/GPRS network using the TCP/IP protocol.

The signal quality can be expressed using the received signal strength indicator (RSSI). The RSSI is often equivalent to the power measured by the receiver [55]. However, several factors can affect RSSI values measured by the receiver. These factors are reflection, diffraction, signal sources, the dynamic environment, and obstacles in the path of radio signal waves. Mo et al. [56] reported that RSSI is a significant packet loss indicator in wireless sensor networks.

As shown in Figure 6, the main subroutine is a part of the program that runs continuously. However, some commands require a response from the service provider, such as the AT+CSQ, AT+CCLK, AT+CGATT, AT+CIPSTART, AT+CIPSEND, among others. The response time (t_{resp}) varied depending on the strength of the RSSI signal. The RSSI stability in outdoor conditions can be affected by temperature, humidity, obstacles, multipath fading effects, distance between the transmitter and receiver, and other noises [18], [57], [58]. Therefore, a digital filter was applied in this study as a simple moving average (SMA) to process the RSSI readings and help interpret them into more reliable data. SMA is suitable for reading RSSI owing to its simplicity despite its settling and response delay [57]. The SMA was used to filter out unwanted noise from the raw RSSI data. The SMA works by taking n RSSI readings to produce an average RSSI reading. Mathematically, the SMA is expressed as follows:

$$y[k] = \frac{1}{N} \sum_{n=0}^{N-1} z[k+n] \quad (1)$$

where z is the raw RSSI value, N is the number of data points before filtering, and y is the filtered RSSI, which is categorized into two groups, namely, signals with good strength (medium/excellent, ME) in the 50–100% range and signals with inadequate strength (medium/bad, MB) in the range of 0–50%.

Figure 8 shows the algorithm for executing AT commands on an SIM7000E modem. The response time limit (t_{LR}) is the maximum time required to wait for a response after executing

the AT command. If a response is obtained when t_{resp} is less than t_{LR} , another AT command ($j = 1, 2, 3 \dots, n$, where n is the last AT command) is automatically executed by first setting t_{LR} for the AT command. If the response is not received even though t_{resp} has exceeded t_{LR} , the same AT command will be re-executed m times without the t_{LR} setting. It then continues with another AT command, if a response is received.

Suppose that a response is not received. In this case, it automatically returned to the initial command from the main subroutine. It is calculated as the data loss in the data transmission cycle and impacts data transmission. Thus, the time spent executing AT commands and waiting for a response will contribute to latency. In other words, this method is non-adaptive (NAL) to variations in t_{resp} value.

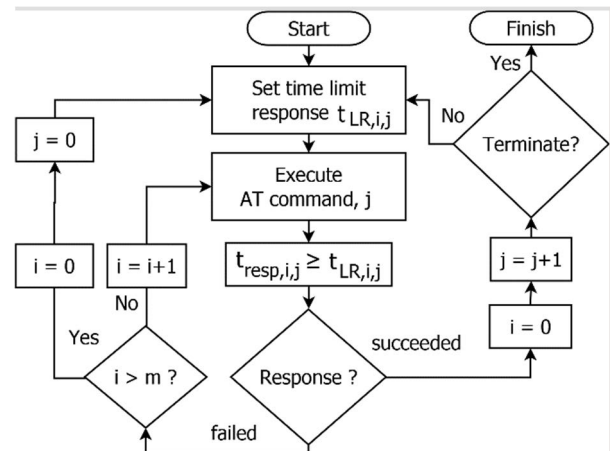


FIGURE 8. SIM7000E GSM/GPRS modem data transmission diagram based on a nonadaptive (NAL) algorithm.

Based on the above problems, this study proposes a simple data transmission algorithm for the SIM7000E modem that behaves adaptively (AL) to variations in t_{resp} values. As shown in Figure 9, the adaptive mechanism of the proposed algorithm updates the t_{LR} value owing to changes in t_{resp} . First, the initial t_{LR} is provided as the default to wait

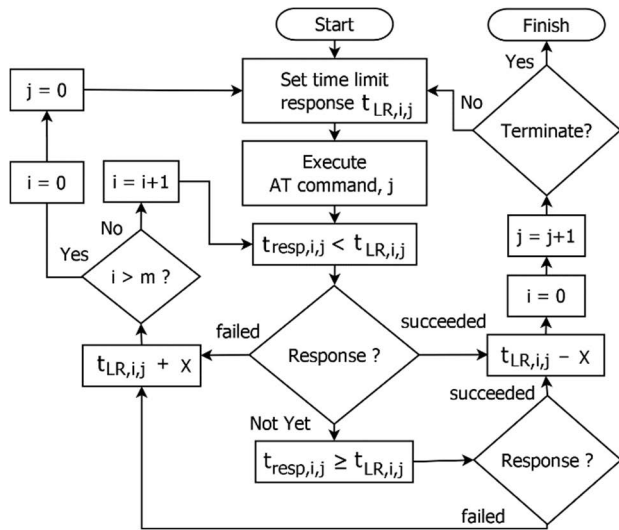


FIGURE 9. SIM7000E GSM/GPRS modem data transmission diagram based on adaptive (AL) algorithm.

for the AT command response. The response obtained when t_{resp} is less than t_{LR} reduces t_{LR} in the next sending cycle by a specific time increment (i.e., X) based on the AT command ($j = 1, 2, 3 \dots, m$). Reducing the t_{LR} value ($t_{LR} - X$) has an effect when the response is not received, accelerating the stage of repeated data transmission. However, if the response is not received when t_{resp} is greater than t_{LR} , the t_{LR} value increases by X ($t_{LR} + X$) at the repeating stage of the AT command ($i = 0, 1, 2, 3, 4, \dots$). The iteration stage of the AT command should be limited to finite iterations, and the variable m is proposed as the maximum iteration limit corresponding to the response time limit and a specific time increment as follows:

$$m = \frac{t_{LR}}{X} - 2 \tag{2}$$

When the response fails, the iteration repeats the AT command if i is less than or equal to m ($i = 0, 1, 2, \dots, m$). In this study, for a maximum of three iterations ($m = 2$), t_{LR} was determined to be 2000 ms based on the response time of AT commands varying from 500 to 1500 ms, such as “AT+CGDCONT?;CGREG?;+CPSI?” and “AT+CGATT=1,” and X is specified in simple algebra, as in (2). Based on the data transmission diagram of the adaptive algorithm, a linear adaptive model was proposed as follows:

$$t_{LR,i,j} = t_{LR,i,j} - X; \quad t_{resp,i,j} < t_{LR,i,j} \tag{3}$$

if response = Succeeded

$$t_{LR,i,j} = t_{LR,i,j} + X; \quad t_{resp,i,j} \geq t_{LR,i,j} \tag{4}$$

if response = failed

where t_{LR} is the default maximum time to wait for a response after executing the AT command, X is a specific time increment, X positively increases t_{LR} when data transmission fails in the previous transmission cycle, and X is negative when

Algorithm 1 Adaptive Performance Stability

```

Input: Signal quality RSSI from AQIMoS
Output: Estimate and determine the most reliable response time limit ( $t_{LR}$ ) based on packet transmission failures
Data: RSSI, packet failed, and latency
Result: Assign and update time response
1: function updatetimerespLimit (RSSI, AT command)
2:  $i = 0, x = 500$  // initial for iteration and specific increment time
3:  $tLim=2000, cTime=0, pTime=0$  //  $tLR$ , current and last time
4: find  $m$ , MA RSSI // limit of iteration and calculate RSSI
5: get  $cTime$  // get the current time in ms
6:  $logic = true$ 
7: if (RSSI > 50 and RSSI <= 100) then
8:  $x = x$ 
9: elseif (RSSI > 0 and RSSI <= 50) then
10:  $x = * 2$ 
11: while  $logic == true$ 
12: execute function AT command,  $j$ 
13: get  $sAT$  // to get the status 'failed' or 'succeeded'
14: get  $tRes$  // time response after AT comm executed
15: if ( $i <= m$ ) then
16: if ( $sAT == failed$  and  $tRes < tLim$ ) then
17:  $tLim = +x$  // in ms
18:  $j++$ 
19: elseif ( $sAT == failed$  and  $tRes >= tLim$ ) then
20:  $tLim = +x$  // in ms
21:  $j++$ 
22: elseif ( $sAT == succeeded$  and  $tRes < tLim$ ) then
23:  $tLim = -x$  // in ms
24: count succeeded response
25: elseif ( $sAT == succeeded$  and  $tRes >= tLim$ ) then
26:  $tLim = -x$  // in ms
27: count failed response
28: elseif ( $i > m$ ) then
29:  $logic = false$ 
30: end
31: get  $pTime$  // get last time in ms
32: calculate the time process based on  $cTime$  and  $pTime$ 
33: end function
34: return updatetimerespLimit for another AT command
35: find latency and packet lost

```

successive data transmissions in the previous transmission cycle reduce t_{LR} .

Algorithm 1 presents the pseudocode of the adaptive program. The output is a command to update the response time limit on the following data transmission cycle. The adaptive algorithm begins by initializing several variables such as the index for iterations, specific time increments, response-time limits, maximum iteration limits, time markers, and RSSI. Next, the maximum iteration limit was defined, RSSI was filtered, and a specific time increment was defined. Finally, the

response time limit was updated, and the latency and packet loss were determined.

Two AT commands are directly related to sending data using the TCP/IP communication protocol in one data transmission cycle: CIPSTART and CIPSEND. Table 4 lists the response times of the two AT commands. For example, in AT+CIPSTART with single-IP mode, the maximum t_{resp} reaches 160 s, whereas the maximum t_{resp} on “AT+CIPSEND” to get a “>” response is 645 s. If the response time limits are set close to both response times, the transmission cycle of the data will be very long, and it will not be possible to set the interval in the future. Therefore, in this study, the initial t_{LR} values in the adaptive and nonadaptive algorithm programs for AT+CIPSTART and “AT+CIPSEND” are each set at 1.5 s and 2 s. The adaptive algorithm updates the t_{LR} according to the conditions by adding and subtracting using a specific time increment.

TABLE 4. Sending data via sim7000e [54].

AT commands	Response	Detail
AT+ CIPSTART	Successful connection: - CONNECT OK connection failed: - CONNECT FAIL	In multi-IP and single -IP, the maximum response time is 75 s and 160 s
AT+ CIPSEND	When there is a connection: - Get sign “>” Successful connection: - SEND OK connection failed: - SEND FAIL	The maximum response time is 645 s and generates a CLOSE response

F. POWER MANAGEMENT

The voltage regulator powered the AQIMoS from a 12 V/7200 mAh valve-regulated lead acid battery. A solar panel with a peak power of 10 watts and maximum voltage of 22 V charges the battery when there is sufficient sunlight. A PWM solar charge controller was used to regulate battery charging, current loading, and battery overcharging.

The power consumption of AQIMoS is intended for use in microcontrollers, modern GSM/GPRS, weather sensors, gas sensors, particulate sensors, regulators, and other electronic components. Maximum power consumption occurs while reading the sensors and transmitting data through a cellular network. The problem with the SIM7000E GPRS modem is related to the need for power supply. Regular modem operation requires several tens of milliamperes, but opening the socket and sending data require a current of approximately 1–2A in milliseconds [59].

G. SERVER AND DATABASE

Servers run on cloud systems managed by Amazon Elastic Compute Cloud (Amazon EC2). The system is run on a Docker basis; thus, it can be automatically reactivated if the server is suddenly down and scaled to improve performance.

The back-end server system was built using the Go programming language, which receives data from a device, processes it, and stores the data in a database. Data processing was performed on the server using the pollutant concentration formula for the air quality index [60].

In addition to running the back-end system and database, the server ran a real-time monitoring dashboard built using HTML, CSS, and JavaScript programming with the ReactJS framework. The dashboard was also integrated with the Google Maps Navigation application to display the measurement location. In addition, as shown in Figure 10, users can easily view the values of all measured parameters on the dashboard via a mobile browser.

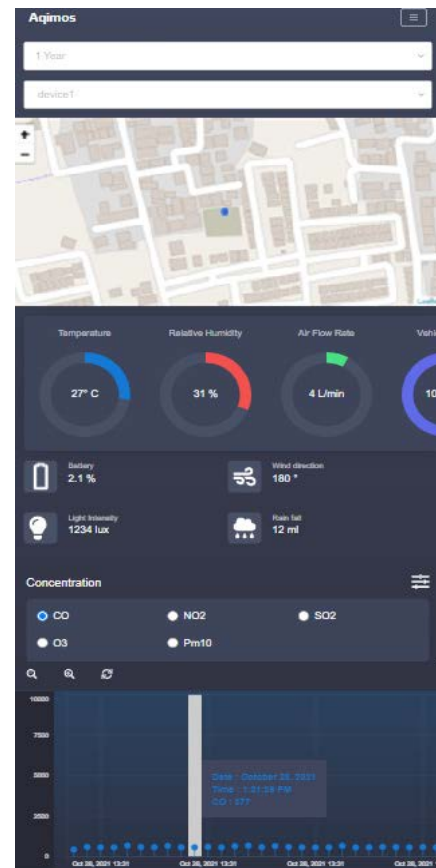


FIGURE 10. Web Application showing pollution at the test site.

H. PERFORMANCE ANALYSIS

System performance measurement is carried out to determine the performance quality of AQIMoS based on quality-of-service parameters, such as latency and packet loss ratio. Latency determines the time required to transmit data from the transmitter to the receiver. Distance, physical media, and long processing times affect latency. Latency is calculated as the difference between the time the device sends data (P_{sd}) and the time the server receives data (P_{rd}) in seconds, as shown in (4). AQIMoS and its servers refer to coordinated universal time (UTC) as a standard of uniformity of seconds

to measure the latency. Equation (4) can be used to estimate the latency between the GSM module and the server.

$$latency = P_{sd} - P_{rd} \tag{5}$$

Packet loss is a parameter that describes the ratio of the number of failed packets received by the receiver (P_L) to the total packets sent by the transmitter. Packets may be lost if the signal strength received at the receiver is lower than the radio sensitivity [61]. The percentage of data packets lost is the ratio of the number of packets that failed to receive the total data sent (P_{TS}), as shown in (6).

$$Packet\ Loss\ Ratio = \frac{P_L}{P_{TS}} \times 100\% \tag{6}$$

AQIMoS always maintains a record of the data packets sent to determine the number of packages sent by the device within a certain period. During the same period, the server logs also show the number of data packets received. The difference between the number of data packets sent by the device and those received by the server is used to calculate the percentage of packet transmission failures within a particular data transmission period.

I. AIR POLLUTANT STANDARD INDEX (ISPU)s

The determination of the daily air quality status is based on ISPU calculations according to Indonesian standards, as shown in (7) [21]. The server calculates the index of pollutant concentration sent from AQIMoS using Table 5 to determine the two breakpoint values, which include the observed concentration (C_p).

$$I_p = \frac{I_{Hi} - I_{Lo}}{BP_{Hi} - BP_{Lo}} (C_p - BP_{Lo}) + I_{Lo} \tag{7}$$

where BP_{Hi} and BP_{Lo} are concentration breakpoint that is the higher and lower than or equal concentrations of the air pollutant, I_{Hi} and I_{Lo} are the AQI values corresponding to those concentration breakpoints, and I_p is the AQI values corresponding to pollutant concentration p .

TABLE 5. Pollutant concentration breakpoint for ISPU.

ISPU	24-h PM ₁₀ μg/m ³	24-h PM _{2.5} μg/m ³	24-h SO ₂ μg/m ³	24-h CO μg/m ³	24-h O ₃ μg/m ³	24-h NO ₂ μg/m ³	24-h HC μg/m ³
0-50	50	15.5	52	4000	120	80	45
51-100	150	55.4	180	8000	235	200	100
101-200	350	150.4	400	15000	400	1130	215
201-300	420	250.4	800	30000	800	2260	432
>300	500	500	1200	45000	1000	3000	648

III. IMPLEMENTATION AND RESULTS

The measurement results are presented in the following section. The results show the calculated power consumption, latency, and packet loss ratio. Power consumption observations were carried out at 50 ms intervals using the INA219 sensor module in a separate system. The SIM7000E module

works in the GPRS mode, and the ripple current usually reaches 2 A that occurs in a short time of approximately 577 μs, and this phenomenon may not be observed.

The signal received by the SIM7000E modem is listed in the RSSI as a unitless number with values ranging from 0 to 31, as presented in Table 6. Signal strength is obtained by executing “AT+CSQ=?.” To test the performance of AQIMoS data delivery, the RSSI filtered using SMA was expressed as a percentage to simplify the interpretation of the signal strength during the test.

TABLE 6. Signal level via at command of sim7000e [54].

RSSI	Units in dBm
0	-115 or less
1	-111
2-30	-110 until -52
31	-52 or greater
99	Not known or not detectable

A. POWER CONSUMPTION

Power consumption is measured during data transmission in the JSON format, where the data size for each transmission cycle is 689 B and 265 B for the body message and header, respectively. In addition, a power meter was installed on the supply line of the SIM7000E module between the input voltage pin and ground to determine the power consumption profile in the transmission process.

The data transmission cycle starts by checking the signal strength (AT+CSQ) until the termination of the TCP connection (AT+CIPCLOSE). The power measurement starts when AQIMoS is turned on, until the data are sent to the server. However, it is interesting to discuss the power consumption during data transmission. As shown in Figure 11, the current ripple appears as some AT commands are executed and messages are received from the server. Current and voltage ripples were recorded using INA219 every 100 ms from 13:27:00:04 to 13:28:00:04 (1-min) for one data transmission cycle displayed in real-time on a computer. Simultaneously, AQIMoS was monitored using a serial monitor to display the executed AT commands and retrieved messages. The most significant current ripple occurs when SIM7000E initiates a TCP connection, sends header and body messages, receives HTTP responses, and terminates the connection. After a study was conducted [49], the larger the data packet sent, the longer it takes for transmission and the greater the power consumption.

Figure 12 shows the difference in the current and voltage ripple patterns from the AQIMoS simulation, which can initially send data but suddenly does not receive a signal and fails to transmit data. The simulation is carried out by removing the antenna on the SIM7000E module so that AQIMoS is ensured that it does not get a signal by getting “99” feedback on the AT+CSQ command. As shown in Figure 12, AQIMoS does not receive a signal and there is no current

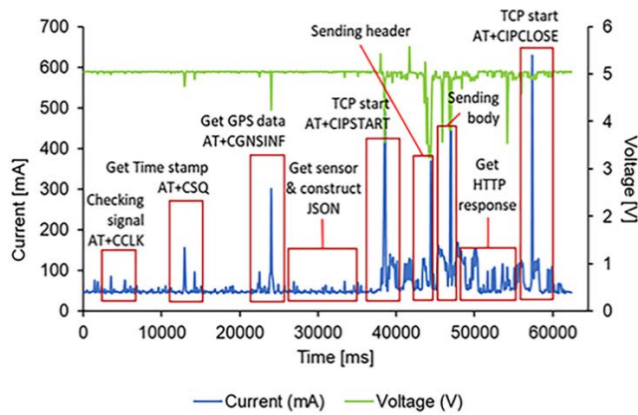


FIGURE 11. Module SIM7000E power consumption profile to sending 954 B in one data transmission cycle.

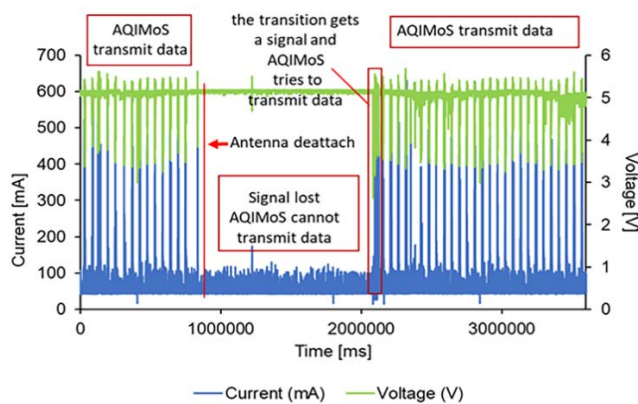


FIGURE 12. The difference in power consumption with the presence and loss of signal on the SIM7000E module.

ripple (950000–2100000 ms). However, a small spike of tens of milliamperes is caused by some AT commands still being executed, such as AT+CSQ and AT+CIPSHUT, to disable GPRS PDP context and AT+CGATT for activation and deactivation of GPRS service. Finally, the antenna was reassembled at 140000 ms, resulting in a signal detected (AT+CSQ response not “99”) and entered a transition state. Subsequently, AT commands for connection to the GPRS service network and data transmission can usually be executed, and an appropriate response can be obtained from the service provider or server.

The power consumption of the AQIMoS device was monitored to determine the power requirements of the system. As shown in Figure 13, the power consumption of the AQIMoS devices is in the range 280–410 mA, and this value is much greater than the power consumption only for the data transmission module. PM sensors and fans are the primary sources of power consumption, whereas gas and weather sensors add only a negligible amount. However, the power consumption of the system is the result of the accumulation of the power consumption of all electronic components, in contrast to that of the AQIMoS device.

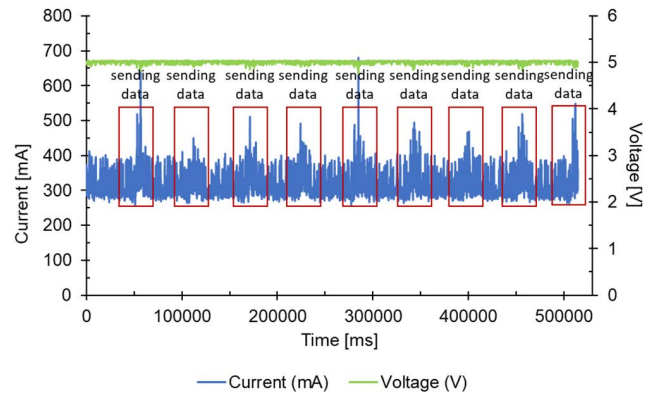


FIGURE 13. AQIMoS device power consumption profile for sending data in minute intervals.

The daily intensity of sunlight during the test affected the output voltage of the solar panel, which subsequently affected the charging of the battery by the solar panel. Figure 14 shows the charge–discharge cycle of the battery based on the ability of the solar panel to harvest solar energy. During the day (06.30 AM to 05.30 PM), solar power is harvested in stages with a solar panel output voltage of 21.25 V. However, at night (06.00 PM to 06.00 AM), the solar panel output voltage is only hundreds of millivolts. Therefore, under cloudy and rainy conditions, battery charging is hampered, and the battery cannot be fully charged at the battery voltage level on June 15, 2022, which did not return to the same battery level as the previous date. Rainy and cloudy conditions during the day for several hours significantly affect battery charging, making it difficult to reach full conditions (12.8–13.0 V).

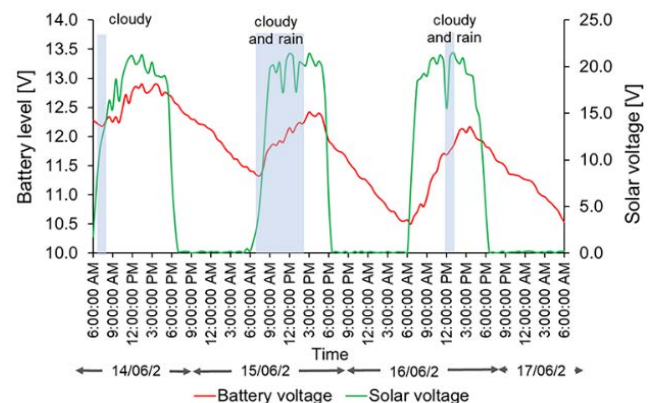


FIGURE 14. Solar battery charge–discharge cycle for three days.

B. TRANSMISSION PERFORMANCE

In this study, to test the performance of the adaptive algorithm, the AQIMoS prototype used in rural and urban areas to obtain RSSI readings on SIM7000E was in the medium/bad (MB) and medium/excellent (ME) categories. Achieving these conditions is important for determining the performance of the AQIMoS prototype of the adaptive algorithm under both conditions.

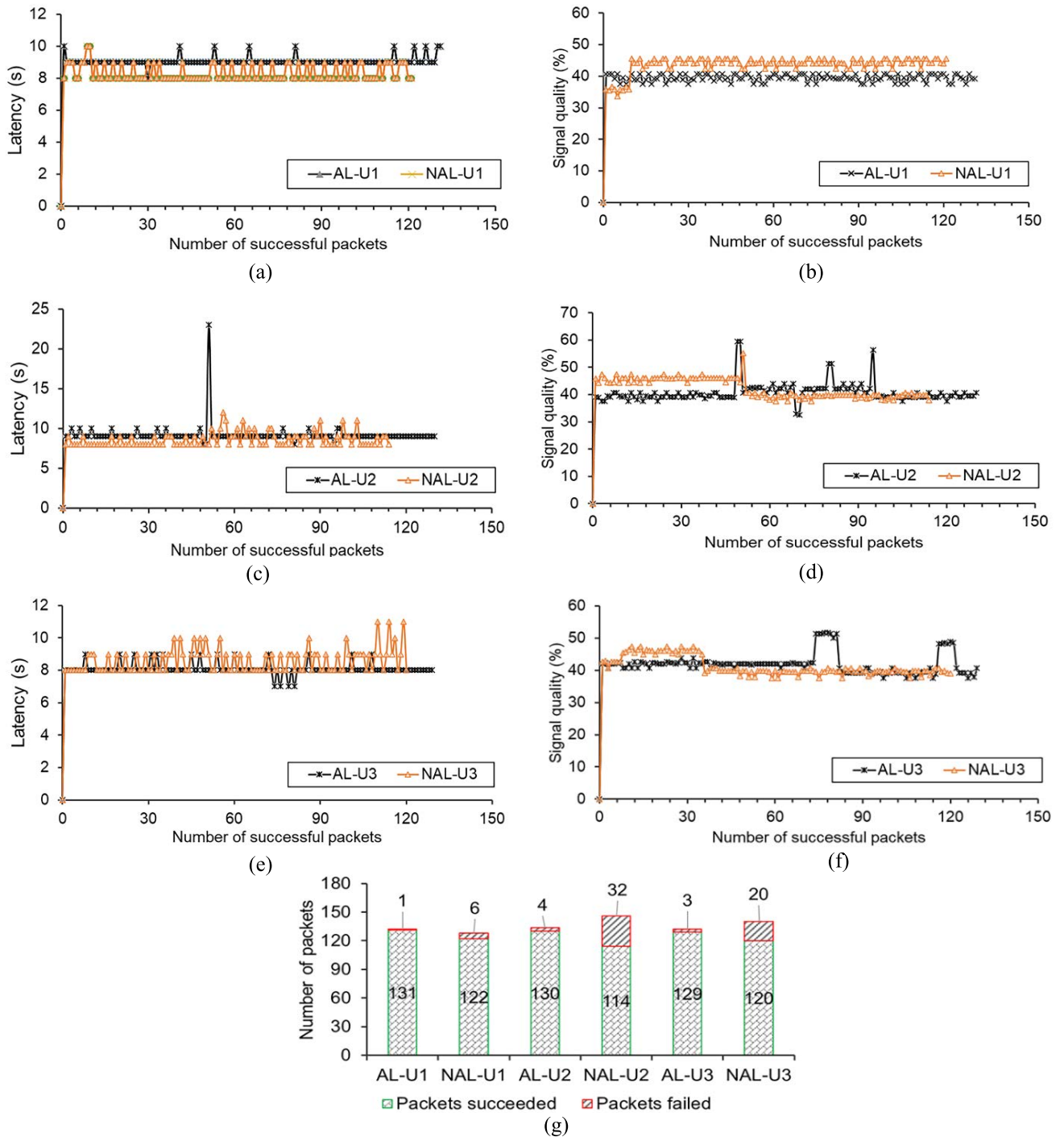


FIGURE 15. Testing result of AQIMoS-A-AL and AQIMoS-B-NAL on MB category signal on (a) latency on U-1, (b) signal level on U-1, (c) latency on U-2, (d) signal level on U-2, (e) level in U-3, (f) signal level on U-3, and (g) packets succeeded and failed to send in each iteration.

The tests were performed using two AQIMoS devices (A and B) designed with the same PCB, electronic components, and voltage source specifications. The test was carried out in two sets, where each set was repeated three times with each repetition for 30 min for each ME and MB signal condition to avoid bias in the test results. The AQIMoS-A device

programmed with the adaptive algorithm (AL), named AQIMoS-A-AL, and the AQIMoS-B device programmed with the nonadaptive algorithm (NAL), named AQIMoS-B-NAL, were tested simultaneously in the first test set. In contrast, the second set of tests was performed by setting AQIMoS-A as NAL and AQIMoS-B as AL.

1) FIRST TEST SET

Fig. 15 shows the results of the first test under the MB cellular signal conditions. Figure 15a, 15c, and 15e show a comparison of the latency by AQIMoS-A-AL and AQIMoS-B-NAL under signal conditions, as shown in Figure 15b, 15d, and 15f for U1, U2, and U3.

Tables 7 and 8 summarize the statistical analyses of the signal levels and latency from the first test set in the MB category. In the MB signal category, the signal level received by the two AQIMoS devices fluctuated in the signal-reading range presented in Table 6. Fluctuations in the signal received by the device caused variations in t_{resp} , affecting the fluctuations in the data transmission latency during the test. In AQIMoS-A-AL devices, changes in t_{resp} can cause the t_{LR} value to be set higher or lower than the initial value, thereby affecting high and low latency. Therefore, the measured latency of the AQIMoS-A-AL device can be smaller or larger than that of the AQIMoS-B-NAL device, as presented in Table 8.

TABLE 7. Signal level in MB category first test set.

Parameters	A		B		A		B	
	AL	NAL	AL	NAL	AL	NAL	AL	NAL
	U1	U1	U2	U2	U3	U3	U3	U3
Mean	39.5	43.8	40.8	42.4	42.0	41.3		
Range	3.1	11.9	27.0	17.6	14.1	9.8		
Minimum	37.6	33.6	32.6	37.6	37.6	37.6		
Maximum	40.8	45.6	59.6	55.2	51.7	47.4		
Count	131	121	130	114	129	120		

TABLE 8. Latency in MB category first test set.

Parameters	A		B		A		B	
	AL	NAL	AL	NAL	AL	NAL	AL	NAL
	U1	U1	U2	U2	U3	U3	U3	U3
Mean	9.1	8.4	9.2	8.6	8.1	8.6		
Range	2.0	2.0	15.0	4.0	2.0	3.0		
Minimum	8.0	8.0	8.0	8.0	7.0	8.0		
Maximum	10.0	10.0	23.0	12.0	9.0	11.0		
Count	131	121	130	114	129	120		

The total amount of data transmitted by AQIMoS-A-AL and AQIMoS-B-NAL differed for each replicate, as shown in Figure 15g. For example, in the U1, U2, and U3 repeats, the total amount of data sent by AQIMoS-A-AL was 132, 134, and 132, respectively. The total data sent by AQIMoS-B-NAL to U1, U2, and U3 were 128, 146, and 140, respectively. The difference in the total data transmitted by the device in each test was due to the different signal reception conditions in each trial. Meanwhile, the difference in the total data sent between AQIMoS-A-AL and AQIMoS-B-NAL in each replication was owing to the adaptive algorithm adjusting the t_{LR} value such that it was possible to obtain a response, although the first AT command execution failed. Meanwhile, in the nonadaptive algorithm, the t_{LR} value is constant, although the

AT command execution is repeated three times at the end. Consequently, the response is still not obtained.

The packet loss ratios of AQIMoS-A-AL for tests U1, U2, and U3 were 0.8%, 3.0%, and 2.3%, respectively. Meanwhile, the packet loss ratios of AQIMoS-B-NAL for the U1, U2, and U3 tests were 4.7%, 21.9%, and 14.3%, respectively. The most significant packet loss ratio occurred in the AQIMoS-B-NAL U2 test of 21.9%, where the percentage was mainly due to failure to receive responses from AT+CCLK and AT+CGSINF.

Fig. 16 shows the results of the first set of tests in the ME category. Figure 16a, 16c, and 16e show a comparison of the latency by AQIMoS-A-AL and AQIMoS-B-NAL under signal conditions, as shown in Figure 16b, 16d, and 16f. Tables 9 and 10 show the statistical analyses of the latency and signal levels. The average signal level received by both devices in each replication was relatively stable, ranging from 82.1% to 86.8%. The average latency of both devices was lower than that of the MB signals.

TABLE 9. Signal level in ME category first test set.

Parameters	A		B		A		B	
	AL	NAL	AL	NAL	AL	NAL	AL	NAL
	U1	U1	U2	U2	U3	U3	U3	U3
Mean	82.5	85.6	82.1	84.4	86.2	86.8		
Range	15.7	12.5	3.1	12.5	12.5	15.7		
Minimum	69.0	78.4	81.4	75.6	84.5	81.5		
Maximum	84.6	90.9	84.5	88.2	97.0	97.2		
Count	147	144	143	140	143	140		

TABLE 10. Latency in ME category first test set.

Parameters	A		B		A		B	
	AL	NAL	AL	NAL	AL	NAL	AL	NAL
	U1	U1	U2	U2	U3	U3	U3	U3
Mean	6.2	7.5	6.7	7.5	6.0	6.5		
Range	5.0	2.0	1.0	1.0	2.0	2.0		
Minimum	5.0	7.0	6.0	7.0	5.0	6.0		
Maximum	10.0	9.0	7.0	8.0	7.0	8.0		
Count	147	144	143	144	143	140		

In the ME signal category, t_{resp} has a lower value of t_{LR} so that the transfer between AT commands becomes fast, causing the time required for data transmission to be faster. In AQIMoS-A-AL, the adaptive algorithm updates the t_{LR} value to half of the initial t_{LR} value if the response is obtained when the t_{resp} value is less than the t_{LR} value. The narrowing of the t_{LR} value is owing to the expectation of a decrease in the signal, resulting in a t_{resp} greater than t_{LR} , which causes the timeout to be achieved faster and the t_{LR} to be updated.

The packet loss ratio analysis was based on the total data sent by the AQIMoS device to the data-acquisition system, as shown in Figure 16. At each iteration, the AQIMoS-A-AL device had a smaller packet loss ratio than that of the AQIMoS-B-NAL device. This is because adaptive algorithms can update t_{LR} when the expected response fails or receives an unexpected response. This adaptive mechanism can increase

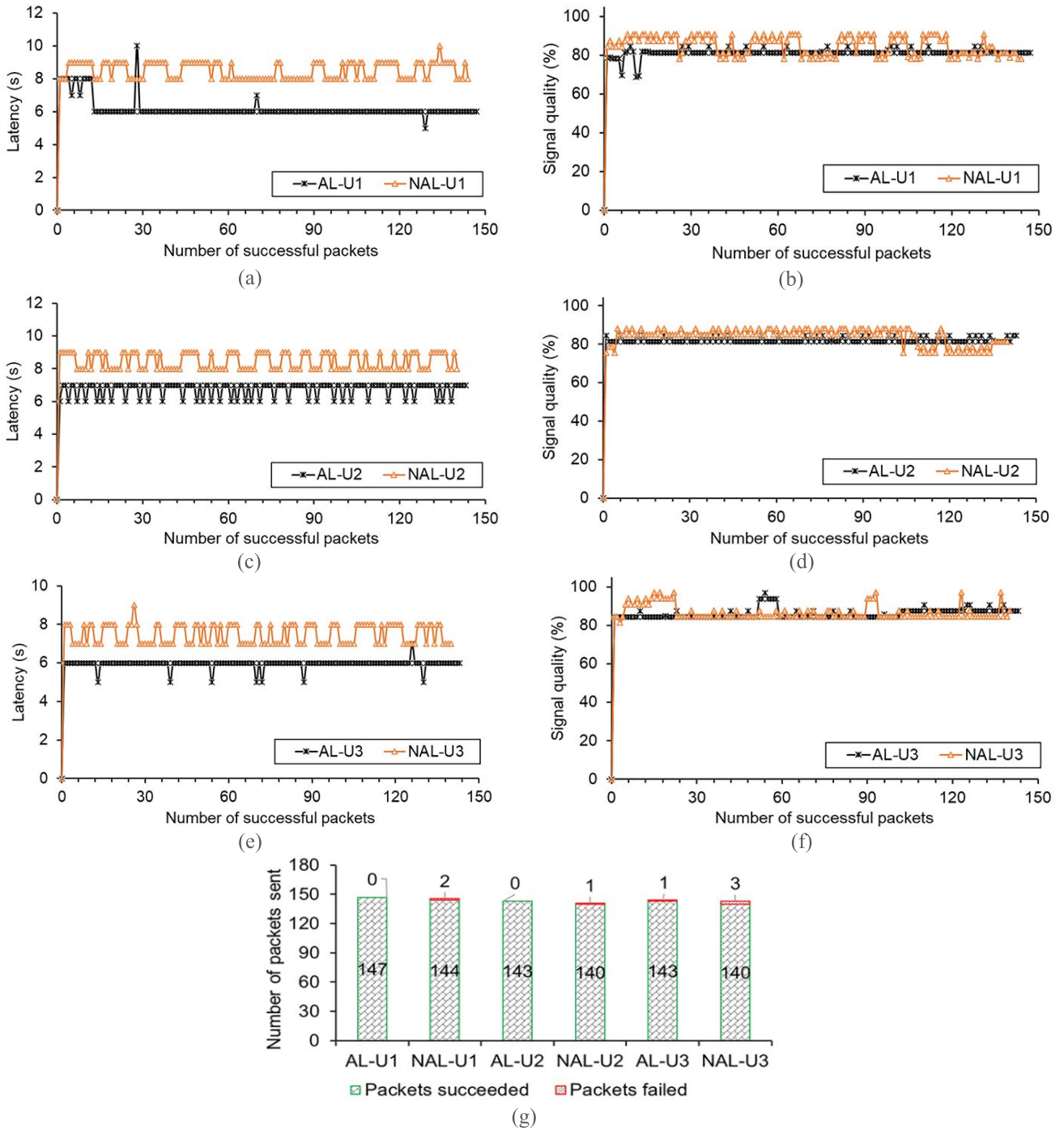


FIGURE 16. Testing result of AQIMoS-A-AL and AQIMoS-B-NAL on ME category signal on (a) latency on U-1, (b) signal level on U-1, (c) latency on U-2, (d) signal level on U-2, (e) level on U-3, (f) signal level on U-3, and (g) packets succeeded and failed to send in each iteration.

the probability of AQIMoS-A-AL obtaining the expected response with a smaller packet loss ratio than the AQIMoS-B-NAL devices. However, when comparing the packet loss ratio in the MB signal category, the packet loss ratio between the AQIMoS-A-AL and AQIMoS-B-NAL devices in the ME signal category was insignificant. This is because under ME signal conditions, the t_{resp} recorded by both devices

was shorter than the t_{resp} recorded during the MB signal conditions.

2) SECOND TEST SET

The second set of tests was conducted to validate the performance differences between AQIMoS devices with and without the adaptive program. In the second test, the AQIMoS-A

device initially inserted with the adaptive program was set as a nonadaptive device and named AQIMoS-A-NAL. In contrast, the native AQIMoS-B program, initially inserted with a nonadaptive device, was configured into an adaptive device, AQIMoS-B-AL.

Figure 17 shows the results of the second test on the MB cellular signal conditions. Figure 17a, 17c, and 17e show a comparison of data transmission latency by AQIMoS-A-NAL and AQIMoS-B-AL under signal conditions, as shown in Figure 17b, 17d, and 17f for U1, U2, and U3 repetitions. Tables 11 and 12 summarize the statistical analyses of the signal levels and latencies of the AQIMoS devices. The average signal levels received by both the devices were the same for each repetition. However, the reception rate of the AQIMoS-A-NAL signal fluctuated during the U3 repetition. Therefore, the AQIMoS-A-NAL latency on U3 fluctuated owing to the fluctuations in the signal received by the device.

As shown in Figure 17g, the packet loss ratio analysis indicates that the AQIMoS-B-AL device has a lower packet loss ratio than AQIMoS-A-NAL because the AQIMoS-B-AL device embedded with an adaptive algorithm can update the t_{LR} value when t_{resp} becomes more extensive owing to the deteriorating signal. Relaxation of the t_{LR} results in increased latency and waiting time to increase the possibility of a response being received by AQIMoS-B-AL, causing the packet loss ratio of AQIMoS-B-AL to be higher than that of AQIMoS-A-NAL. A constant t_{LR} value cannot increase the probability of data transmission owing to changes in t_{resp} value, particularly when t_{resp} increases.

TABLE 11. Signal level in MB category second test set.

Parameters	B		A		B		A	
	AL	NAL	AL	NAL	AL	NAL	AL	NAL
	U1	U1	U2	U2	U3	U3	U3	U3
Mean	39.9	37.8	42.0	42.9	38.0	36.5		
Range	21.6	12.5	2.8	13.7	6.3	31.1		
Minimum	19.9	27.6	40.6	31.2	34.3	24.8		
Maximum	41.4	40.2	43.4	44.9	40.6	55.8		
Count	131	125	136	133	137	118		

TABLE 12. Latency in MB category in second test set.

Parameters	B		A		B		A	
	AL	NAL	AL	NAL	AL	NAL	AL	NAL
	U1	U1	U2	U2	U3	U3	U3	U3
Mean	8.0	8.2	7.9	9.4	7.8	9.6		
Range	6.0	2.0	2.0	9.0	2.0	9.0		
Minimum	7.0	8.0	7.0	9.0	7.0	8.0		
Maximum	13.0	10.0	9.0	18.0	9.0	17.0		
Count	131	125	136	133	137	118		

Figure 18 shows the results of the second test for the ME signal category. Figures 18a, 18c, and 18e show the results of the AQIMoS-A-NAL and AQIMoS-B-AL latency tests, respectively. Figures 18b, 18d, and 18f show the signal levels obtained during the tests. The experimental results show that

the signal levels received by AQIMoS-A-NAL and AQIMoS-B-AL were not significantly different based on the statistical analysis presented in Table 13. Nonetheless, the signal level fluctuated during the test, as shown in Figures 18b, 18d, and 18f. Fluctuations in the signal level received by both devices cause t_{resp} to fluctuate and potentially affect the latency.

Figures 18a, 18c, and 18e show that the actual latencies recorded by AQIMoS-A-NAL and AQIMoS-B-AL fluctuated during the test. As shown in Table 14, the statistical analysis results indicate that the AQIMoS-A-NAL latency is lower than that of AQIMoS-B-AL. As shown in Figure 18g, the total number of packets sent by the two devices did not differ significantly because t_{resp} was smaller than t_{LR} set for AQIMoS-A-NAL and AQIMoS-B-AL. Another result is that even though the signal strength fluctuates, the AQIMoS-B-AL device can maintain the data transmission process, which is indicated by the low packet loss ratio for each repetition.

TABLE 13. Signal level in ME category second test set.

Parameters	B		A		B		A	
	AL	NAL	AL	NAL	AL	NAL	AL	NAL
	U1	U1	U2	U2	U3	U3	U3	U3
Mean	82.7	84.0	88.3	83.9	87.5	87.4		
Range	36.1	12.5	12.5	24.5	28.2	21.9		
Minimum	58.0	75.2	81.5	66.5	69.0	75.2		
Maximum	94.0	87.8	94.0	90.9	97.2	97.2		
Count	150	136	152	134	155	140		

TABLE 14. Latency in ME category second test set.

Parameters	B		A		B		A	
	AL	NAL	AL	NAL	AL	NAL	AL	NAL
	U1	U1	U2	U2	U3	U3	U3	U3
Mean	6.7	7.1	6.0	7.2	6.2	7.1		
Range	3.0	1.0	2.0	1.0	3.0	2.0		
Minimum	5.0	7.0	5.0	7.0	5.0	6.0		
Maximum	8.0	8.0	7.0	8.0	8.0	8.0		
Count	150	136	152	134	155	140		

The fluctuation of the RSSI in each test is another result that needs to be discussed from the second test result. RSSI spikes still appear even though the SMA has filtered it with a 7-point data sample ($n = 7$). This can be overcome by using a more significant number of data sample points; however, this can increase deposition and response delays. Another alternative is to use a digital filter, such as the Kalman filter, which has a better noise reduction capability and lower response delay than SMA to eliminate RSSI spikes [62]. Significant RSSI changes can cause signal strength categorization errors (MB or ME category), especially for signal strengths of approximately 50%, affecting t_{LR} . However, a significant difference in the performance of adaptive and non-adaptive algorithms is shown in the packet loss analysis under MB conditions, where devices with adaptive programs have a lower packet loss than non-adaptive devices.

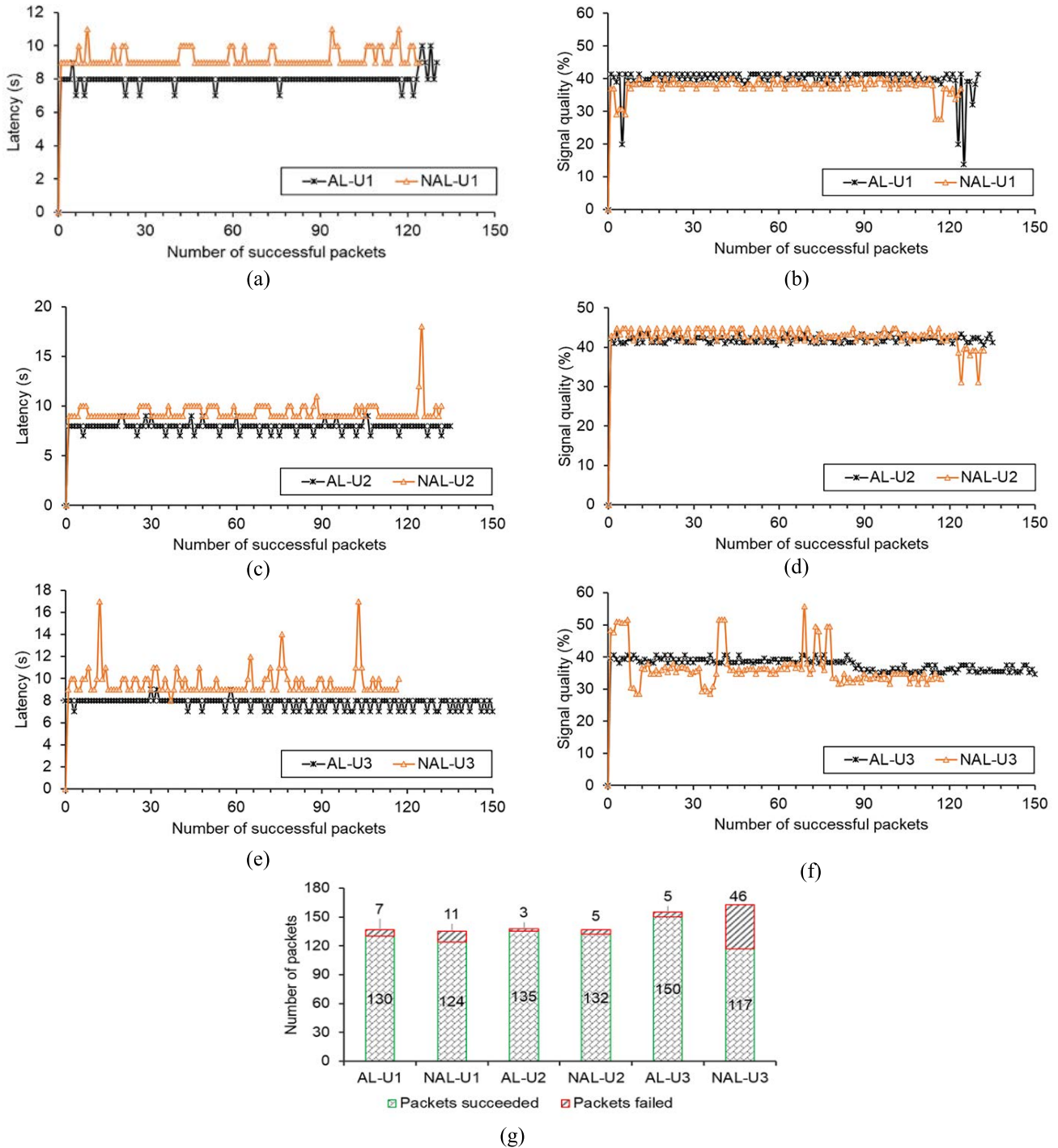


FIGURE 17. Testing result of AQIMoS-A-NAL and AQIMoS-B-AL on MB category signal on (a) latency on U-1, (b) signal level on U-1, (c) latency on U-2, (d) signal level in U-2, (e) level in U-3, (f) signal level in U-3, and (g) packets succeeded and failed to send in each iteration.

Meanwhile, there was no significant difference in packet loss under the ME conditions of the two devices. However, in MB conditions, AQIMoS devices tend to be constrained to send packets and receive responses compared to ME conditions because at low RSSI levels, there is a decrease in the data rate and an increase in packet loss [19], [61]. Therefore, on

nonadaptive devices, packet loss in the MB condition experienced a significant increase compared to the ME condition. For adaptive devices in the MB and ME conditions, there is a t_{LR} adjustment by adding and subtracting certain time increments that can reduce packet loss but can increase latency, which is a weakness of the linear adaptive model, especially

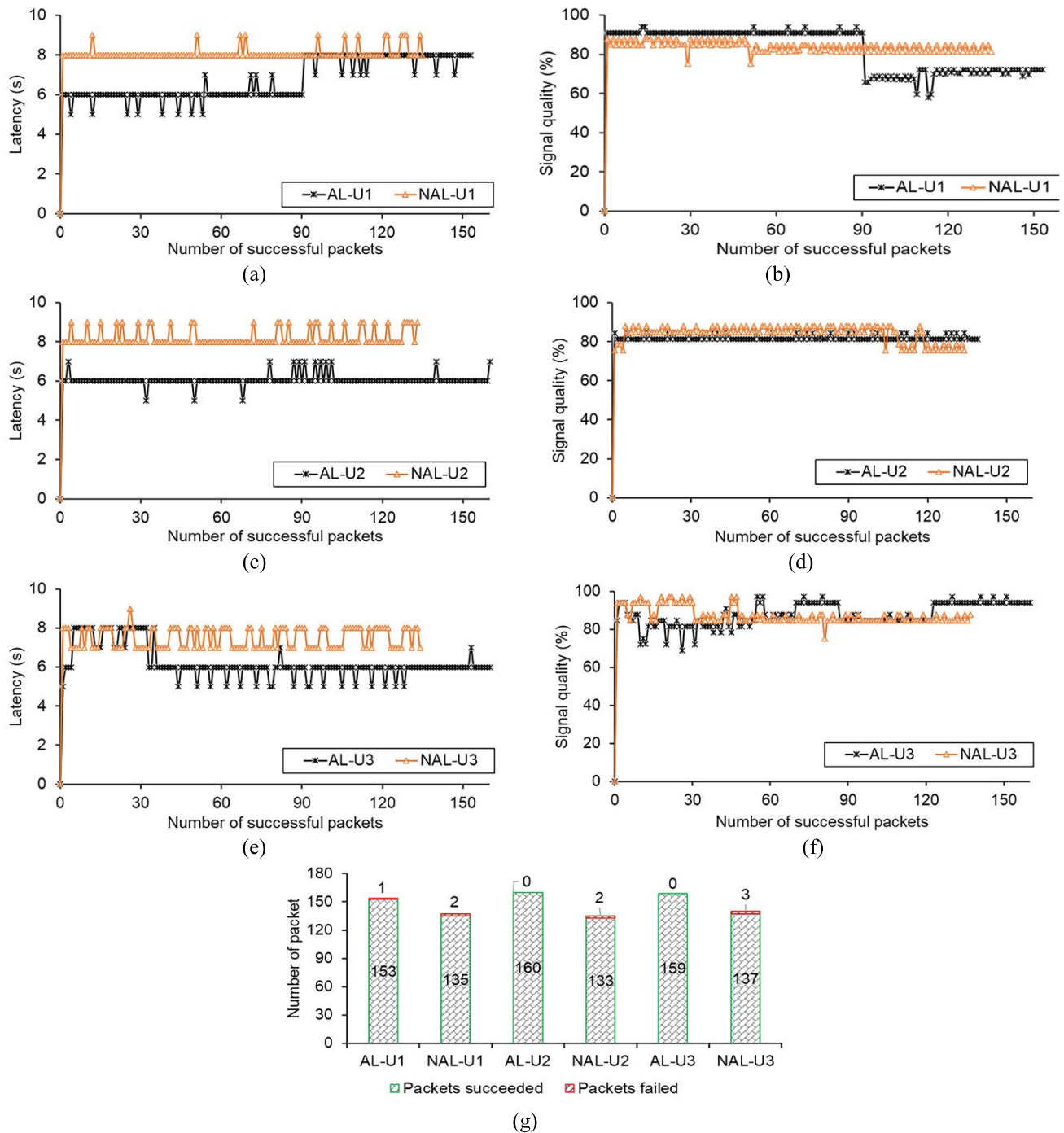


FIGURE 18. Testing result of AQIMoS-A-NAL and AQIMoS-B-AL on ME category signal on (a) latency on U-1, (b) signal level on U-1, (c) latency on U-2, (d) signal level in U-2, (e) level in U-3, (f) signal level in U-3, and (g) packets succeeded and failed to send in each iteration.

in MB conditions. In the future, to anticipate these weaknesses, RSSI readings with different levels of variation will be adaptively filtered with different filtering levels to build a graded RSSI classification method (above or below 50%). The RSSI categorization can be used to determine the specific time increment value for each RSSI classification and build an adaptive mechanism for determining the t_{LR} .

C. PERFORMANCE TESTING

The AQIMoS field test to show the ability of the device to measure pollutants in real-world conditions, a simple setup was performed, i.e., the AQIMoS deployment location for testing was determined in an area close to Atang Senjaya Airport, Bogor City. This location was chosen because it has a high level of traffic owing to the large number of motorized

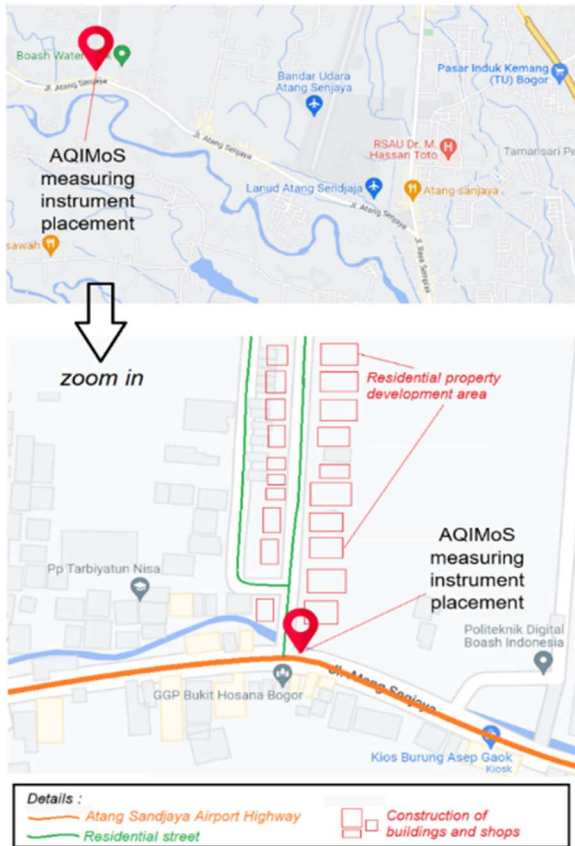


FIGURE 19. The location for testing the AQIMoS device is about 2 km from Atang Senjaya Airport, Bogor City.

vehicles, especially diesel trucks carrying sand, as shown in Figure 19. In addition, safety, and permit placement of the monitoring equipment during the test were considered. The complete experimental results regarding the application of AQIMoS require further testing.

Pollutant sensor data sent from AQIMoS to the server were downloaded using a web application and averaged into hourly data, as shown in Figure 20. The average hourly pollutant concentration data were used to determine the fluctuations in the concentration pattern change in the measurement time range. To determine the daily air quality status during the measurement, the pollutant concentration was averaged every 24-h from the start of the measurement onwards. The 24-h average concentration was used to calculate the air pollutant standard index (ISPU) to obtain the ISPU category. The ISPU for June 13–14, 14–15, 15–16, and 16–17, 2022, were 66, 82, 60, and 72, respectively, of which the first three ISPUs were dominated by PM_{2.5} and the last ISPU by PM₁₀. Thus, all the air quality statuses based on the ISPU category were moderate.

The critical technical point in determining the location of air quality observations using AQIMoS is another interesting point to discuss, considering the range of cellular signals that support GSM/GPRS communication. AQIMoS placed in an

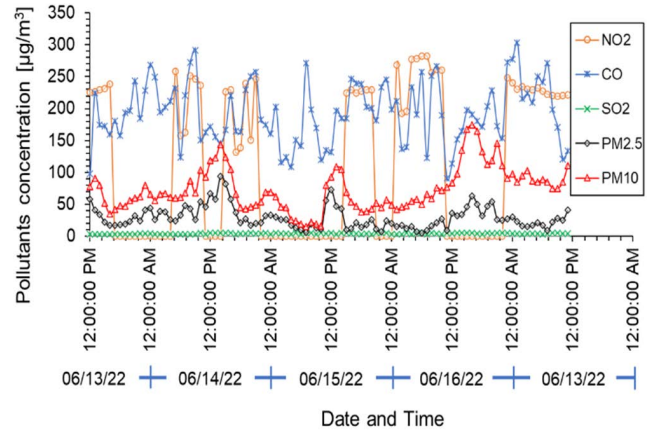


FIGURE 20. Measurement of pollutant concentration for 4 days by AQIMoS.

area with no cellular signal cannot connect to the internet and fails to send packets to the server. Therefore, from the outset, locations to monitor the availability of cellular signals must be identified, considering environmental aspects such as industrial areas, mining areas, and congested urban roads. The device can be used anywhere if a cellular signal is available.

The development of remote monitoring technology, which is becoming increasingly advanced along with the implementation of the Internet of Things, has increased the use of modems and the expansion of cellular networks available in remote areas. This has positively impacted the development of modern GPRS technology that can implement TCP/IP protocols and is supported by general input and output, the Modbus protocol, and GPS, which can be integrated with controllers capable of static or mobile monitoring systems.

However, in contrast to its advantages, the GPRS modem has disadvantages related to the operational cost of data transmission. This problem becomes more prominent and severe owing to the number of nodes deployed. An alternative solution to reduce costs is to set a data-transmission interval. In the future, this interval setting can also be adjusted according to the supply voltage level to adaptively reduce the power consumption. However, this solution must be studied with respect to the temporal resolution of air quality data. Another solution is to use a GPRS modem as an interface for the entire wireless sensor network, as proposed by Gutiérrez et al., Wang et al., and Schiavo [63], [64], [65]. Wireless sensor networks can be built using radio communications such as Zigbee, LoRa, or Wi-Fi protocols.

IV. CONCLUSION

This paper develops and tests a linear adaptive model for the RSSI signal at the AQIMoS (Mobile Air Quality IPB Monitoring System) sensor node based on GSM/GPRS cellular communication. The proposed model can adaptively adjust the response time limit based on the RSSI and

response-receiving status to improve data transmission performance. The results show that by applying the proposed method, devices with adaptive programs have a much lower packet loss ratio than nonadaptive devices, especially when the signal level is below 50% (MB). However, at signal levels below and above 50% (ME), there are conditions where adaptive devices have much greater latency than nonadaptive devices because of the repetition of the data transmission process and added response time limit with a specific increment time. In the future, it will be necessary to categorize signal strength based on variations in RSSI so that several other signal categories can be tested to increase the effectiveness of setting the response time limit. In addition, digital filters can also use the Kalman filter, which has a better ability to reduce RSSI noise and a lower response delay than the moving average. Moreover, performance tests must be conducted in the long term to demonstrate the stability of the overall system performance.

REFERENCES

- [1] P. K. Hopke, S. S. Hashemi Nazari, M. Hadei, M. Yarahmadi, M. Kermani, E. Yarahmadi, and A. Shahsavani, "Spatial and temporal trends of short-term health impacts of PM_{2.5} in Iranian cities; a modelling approach (2013–2016)," *Aerosol Air Quality Res.*, vol. 18, no. 2, pp. 497–504, 2018, doi: 10.4209/aaqr.2017.09.0325.
- [2] M. Iriti, P. Piscitelli, E. Missoni, and A. Miani, "Air pollution and health: The need for a medical reading of environmental monitoring data," *Int. J. Environ. Res. Public Health*, vol. 17, no. 7, p. 2174, Mar. 2020, doi: 10.3390/ijerph17072174.
- [3] M. Kowalska, M. Skrzypek, M. Kowalski, and J. Cyrus, "Effect of NO_x and NO₂ concentration increase in ambient air to daily bronchitis and asthma exacerbation, Silesian Voivodeship in Poland," *Int. J. Environ. Res. Public Health*, vol. 17, no. 3, pp. 1–9, 2020, doi: 10.3390/ijerph17030754.
- [4] S. Ahmed, "Air pollution and its impact on agricultural crops in developing countries—A review," *J. Anim. Plant Sci.*, vol. 25, no. 3, pp. 297–302, 2015.
- [5] P. Rafaj, G. Kiesewetter, Timur Gül, W. Schöpp, J. Cofala, Z. Klimont, P. Purohit, C. Heyes, M. Amann, J. Borken-Kleeefeld, and L. Cozzi, "Outlook for clean air in the context of sustainable development goals," *Global Environ. Change*, vol. 53, pp. 1–11, Nov. 2018, doi: 10.1016/j.gloenvcha.2018.08.008.
- [6] Government of the Republic of Indonesia. (2020). *Regulation of the Minister of Environment and Forestry of the Republic of Indonesia no. 14, of 2020 Concerning the Air Pollution Standard Index*. [Online]. Available: <https://peraturan.bpk.go.id/Home/Download/156214/PermenLHKNNomor14Tahun2020.pdf>
- [7] G. Zhao, G. Huang, H. He, and Q. Wang, "Innovative spatial-temporal network modeling and analysis method of air quality," *IEEE Access*, vol. 7, pp. 26241–26254, 2019, doi: 10.1109/ACCESS.2019.2900997.
- [8] A. Bagula, M. Zennaro, G. Inggs, S. Scott, and D. Gascon, "Ubiquitous sensor networking for development (USN4D): An application to pollution monitoring," *Sensors*, vol. 12, no. 1, pp. 391–414, Jan. 2012, doi: 10.3390/s120100391.
- [9] M. Rahmat, W. Maulina, Isnaeni, D. Y. N. Miftah, N. Sukmawati, E. Rustami, M. Azis, K. B. Seminar, A. S. Yuwono, Y. H. Cho, and H. Alatas, "Development of a novel ozone gas sensor based on sol-gel fabricated photonic crystal," *Sens. Actuators A, Phys.*, vol. 220, pp. 53–61, Dec. 2014, doi: 10.1016/j.sna.2014.09.020.
- [10] M. Rahmat, W. Maulina, E. Rustami, M. Azis, D. R. Budiarti, K. B. Seminar, A. S. Yuwono, and H. Alatas, "Performance in real condition of photonic crystal sensor based NO₂ gas monitoring system," *Atmos. Environ.*, vol. 79, pp. 480–485, Nov. 2013, doi: 10.1016/j.atmosenv.2013.05.057.
- [11] M. Rahmat, M. Azis, E. Rustami, W. Maulina, K. B. Seminar, A. S. Yuwono, and H. Alatas, "Low cost configuration of data acquisition system for wireless sensor network," *Int. J. Eng. Technol.*, vol. 12, no. 2, pp. 1–10, Apr. 2012.
- [12] H. Alatas, H. Mayditia, H. Hardhienata, A. A. Iskandar, and M. O. Tjia, "Single-frequency refractive index sensor based on a finite one-dimensional photonic crystals with two defects," *Jpn. J. Appl. Phys.*, vol. 45, no. 8B, pp. 6754–6758, Aug. 2006, doi: 10.1143/JJAP.45.6754.
- [13] M. Iqbal, M. Fuad, H. Sukoco, and H. Alatas, "Hybrid tree-like mesh topology as new wireless sensor network platform," *Telkomnika Telecommun. Comput. Electron. Control.*, vol. 14, no. 3, pp. 1166–1174, 2016, doi: 10.12928/TELKOMNIKA.v14i3.2279.
- [14] A. R. Al-Ali, I. Zualkernan, and F. Aloul, "A mobile GPRS-sensors array for air pollution monitoring," *IEEE Sensors J.*, vol. 10, no. 10, pp. 1666–1671, Oct. 2010, doi: 10.1109/JSEN.2010.2045890.
- [15] I. Gryech, Y. Ben-Aboud, B. Guermah, N. Sbihi, M. Ghogho, and A. Kobbane, "Moreair: A low-cost urban air pollution monitoring system," *Sensors*, vol. 20, no. 4, pp. 1–24, 2020, doi: 10.3390/s20040998.
- [16] S. Dhingra, R. B. Madda, A. H. Gandomi, R. Patan, and M. Daneshmand, "Internet of Things mobile-air pollution monitoring system (IoT-Mobair)," *IEEE Internet Things J.*, vol. 6, no. 3, pp. 5577–5584, Jun. 2019, doi: 10.1109/JIOT.2019.2903821.
- [17] A. Velasco, R. Ferrero, F. Gandino, B. Montrucchio, and M. Rebaudengo, "A mobile and low-cost system for environmental monitoring: A case study," *Sensors*, vol. 16, no. 5, p. 710, May 2016, doi: 10.3390/s16050710.
- [18] S.-H. Fang and Y.-H. S. Yang, "The impact of weather condition on radio-based distance estimation: A case study in GSM networks with mobile measurements," *IEEE Trans. Veh. Technol.*, vol. 65, no. 8, pp. 6444–6453, Aug. 2016, doi: 10.1109/TVT.2015.2479591.
- [19] S. Xiao, A. Dhamdhere, V. Sivaraman, and A. Burdett, "Transmission power control in body area sensor networks for healthcare monitoring," *IEEE J. Sel. Areas Commun.*, vol. 27, no. 1, pp. 37–48, Jan. 2009, doi: 10.1109/JSAC.2009.090105.
- [20] A. Olesiński and Z. Piotrowski, "An adaptive energy saving algorithm for an RSSI-based localization system in mobile radio sensors," *Sensors*, vol. 21, no. 12, p. 3987, Jun. 2021, doi: 10.3390/s21123987.
- [21] M. Azis, E. Rustami, W. Maulina, M. Rahmat, H. Alatas, and K. Seminar, "Measuring air pollutant standard index (ISPU) with photonics crystal sensor based on wireless sensor network (WSN)," in *Proc. 2nd Int. Conf. Instrum., Commun., Inf. Technol., Biomed. Eng.*, Nov. 2011, pp. 348–351, doi: 10.1109/ICICI-BME.2011.6108656.
- [22] S. Ali, T. Glass, B. Parr, J. Potgieter, and F. Alam, "Low cost sensor with IoT LoRaWAN connectivity and machine learning-based calibration for air pollution monitoring," *IEEE Trans. Instrum. Meas.*, vol. 70, pp. 1–11, 2021, doi: 10.1109/TIM.2020.3034109.
- [23] K. Zheng, S. Zhao, Z. Yang, X. Xiong, and W. Xiang, "Design and implementation of LPWA-based air quality monitoring system," *IEEE Access*, vol. 4, pp. 3238–3245, 2016, doi: 10.1109/ACCESS.2016.2582153.
- [24] E. G. Snyder, T. H. Watkins, P. A. Solomon, E. D. Thoma, R. W. Williams, G. S. W. Hagler, D. Shelow, D. A. Hindin, V. J. Kilaru, and P. W. Preuss, "The changing paradigm of air pollution monitoring," *Environ. Sci. Technol.*, vol. 47, no. 20, pp. 11369–11377, 2013, doi: 10.1021/es4022602.
- [25] L. Spinelle, M. Gerboles, M. Alexandre, and F. Bonavitaola, "Evaluation of metal oxides sensors for the monitoring of O₃ in ambient air at Ppb level," *Chem. Eng. Trans.*, vol. 54, pp. 319–324, Sep. 2016, doi: 10.3303/CET1654054.
- [26] SGXsensortech. (2015). *The MiCS-6814 is a Compact MOS Sensor With Three Fully Independent Sensing Elements on One Package Revision 8*. [Online]. Available: https://www.sgxsensortech.com/content/uploads/2015/02/1143_Datasheet-MiCS-6814-rev-8.pdf
- [27] *MQ-7 Gas Sensor Datasheet*, Hanwei Electronics, China, vol. 1, 2016, pp. 3–5. [Online]. Available: <https://www.sparkfun.com/datasheets/Sensors/Biometric/MQ-7.pdf>
- [28] (2015). *Hydrogen Sulfide Gas Sensor (Model: MQ136)*. Zhengzhou. [Online]. Available: [https://www.winsen-sensor.com/d/files/PDF/SemiconductorGasSensor/MQ136\(Ver1.4\)-Manual.pdf](https://www.winsen-sensor.com/d/files/PDF/SemiconductorGasSensor/MQ136(Ver1.4)-Manual.pdf)
- [29] M. Badura, P. Batog, A. Drzeniecka-Osiadacz, and P. Modzel, "Evaluation of low-cost sensors for ambient PM_{2.5} monitoring," *J. Sensors*, vol. 2018, pp. 1–16, Oct. 2018, doi: 10.1155/2018/5096540.
- [30] T. Migos, I. Christakis, K. Moutzouris, and I. Stavarakas, "On the evaluation of low-cost PM sensors for air quality estimation," in *Proc. 8th Int. Conf. Modern Circuits Syst. Technol. (MOCAST)*, May 2019, pp. 1–4, doi: 10.1109/MOCAST.2019.8742041.
- [31] A. Y. P. Wardoyo, H. A. Dharmawan, M. Nurhuda, and E. T. P. Adi, "Optimization of PM_{2.5} measurement system using Nova SDS011 sensor," *J. Phys., Conf.*, vol. 1428, no. 1, Jan. 2020, Art. no. 012053, doi: 10.1088/1742-6596/1428/1/012053.

- [32] M. Budde, A. D. Schwarz, T. Müller, B. Laquai, N. Streibl, G. Schindler, Marcel Köpke, T. Riedel, A. Dittler, and M. Beigl, "Potential and limitations of the low-cost SDS011 particle sensor for monitoring urban air quality," in *Proc. 3rd Int. Conf. Atmos. Dust (DUST)*, 2018, pp. 6–12, doi: [10.14644/dust.2018.002](https://doi.org/10.14644/dust.2018.002).
- [33] G. Marques, "A cost-effective air quality supervision solution for enhanced living environments through the Internet of Things," *Electronics*, vol. 8, no. 2, pp. 1–16, 2019, doi: [10.3390/electronics8020170](https://doi.org/10.3390/electronics8020170).
- [34] A. N. Abdullah, K. Kamarudin, S. M. Mamduh, and A. H. Adom, "Development of MOX gas sensors module for indoor air contaminant measurement," *IOP Conf. Mater. Sci. Eng.*, vol. 705, no. 1, 2019, Art. no. 012029, doi: [10.1088/1757-899X/705/1/012029](https://doi.org/10.1088/1757-899X/705/1/012029).
- [35] S. Duangsuwan and P. Jamjareekulgarn, "Development of drone real-time air pollution monitoring for mobile smart sensing in areas with poor accessibility," *Sensors Mater.*, vol. 32, no. 2, pp. 511–520, 2020.
- [36] P. Purwanto, S. Suryono, and S. Sunarno, "Design of air quality monitoring system based on web using wireless sensor network," *J. Phys., Conf.*, vol. 1295, no. 1, Sep. 2019, Art. no. 012043, doi: [10.1088/1742-6596/1295/1/012043](https://doi.org/10.1088/1742-6596/1295/1/012043).
- [37] T. N. T. Nguyen, D. V. Ha, T. N. N. Do, V. H. Nguyen, X. T. Ngo, V. H. Phan, N. D. Nguyen, and Q. H. Bui, "Air pollution monitoring network using low-cost sensors, a case study in Hanoi, Vietnam," *IOP Conf. Earth Environ. Sci.*, vol. 266, no. 1, 2019, Art. no. 012017, doi: [10.1088/1755-1315/266/1/012017](https://doi.org/10.1088/1755-1315/266/1/012017).
- [38] M. Pavanani and K. K. Kumar, "Monitoring real-time urban sulphur dioxide and ammonia emissions using the wireless sensor networks," *ARNJ. Eng. Appl. Sci.*, vol. 14, no. 20, pp. 3504–3508, 2019.
- [39] H. Y. Liu, P. Schneider, R. Haugen, and M. Vogt, "Performance assessment of a low-cost PM_{2.5} sensor for a near four-month period in Oslo, Norway," *Atmosphere*, vol. 10, no. 2, pp. 1–19, 2019, doi: [10.3390/atmos10020041](https://doi.org/10.3390/atmos10020041).
- [40] L. Bai, J. Wang, X. Ma, and H. Lu, "Air pollution forecasts: An overview," *Int. J. Environ. Res. Public Health*, vol. 15, no. 4, pp. 1–44, 2018, doi: [10.3390/ijerph15040780](https://doi.org/10.3390/ijerph15040780).
- [41] M. Czarnačka and J. Nidzgorzka-Lencewicz, "Impact of weather conditions on winter and summer air quality," *Int. Agrophysics*, vol. 25, no. 1, pp. 7–12, 2011.
- [42] D. J. Jacob and D. A. Winner, "Effect of climate change on air quality," *Atmos. Environ.*, vol. 43, no. 1, pp. 51–63, 2009, doi: [10.1016/j.atmosenv.2008.09.051](https://doi.org/10.1016/j.atmosenv.2008.09.051).
- [43] J. Seo, D.-S.-R. Park, J. Y. Kim, D. Youn, Y. B. Lim, and Y. Kim, "Effects of meteorology and emissions on urban air quality: A quantitative statistical approach to long-term records (1999–2016) in Seoul, South Korea," *Atmos. Chem. Phys.*, vol. 18, no. 21, pp. 16121–16137, Nov. 2018, doi: [10.5194/acp-18-16121-2018](https://doi.org/10.5194/acp-18-16121-2018).
- [44] S-LABS. (2014). *Si7021-A10 I2C Humidity and Temperature Sensor features Applications Description*. [Online]. Available: <https://cdn.sparkfun.com/datasheets/Sensors/Weather/Si7021.pdf>
- [45] Freescale Semiconductor. (2011). *P²C Precision Altimeter MPL3115A2*. [Online]. Available: <https://cdn.sparkfun.com/datasheets/Sensors/Pressure/MPL3115A2.pdf>.
- [46] Argent Data System. (2014). *Weather Sensor Assembly p/n 80422*. [Online]. Available: https://www.argentdata.com/files/80422_datasheet.pdf
- [47] R. Purbakawaca, A. S. Yuwono, S. K. Saptomo, K. B. Seminar, I. D. M. Subrata, M. Rahmat, and H. Alatas, "Measurement of PM₁₀ concentration using hybrid cyclone separator and particle counter," *IOP Conf. Earth Environ. Sci.*, vol. 622, no. 1, pp. 0–11, 2021, doi: [10.1088/1755-1315/622/1/012025](https://doi.org/10.1088/1755-1315/622/1/012025).
- [48] A. Kadri, E. Yaacoub, M. Mushtaha, and A. Abu-Dayya, "Wireless sensor network for real-time air pollution monitoring," in *Proc. 1st Int. Conf. Commun., Signal Process., Appl. (ICCSA)*, Feb. 2013, pp. 1–5, doi: [10.1109/ICCSA.2013.6487323](https://doi.org/10.1109/ICCSA.2013.6487323).
- [49] V. Prochazka, P. Kubalik, and H. Kubatova, "Low power wireless data transfer for Internet of Things: GSM network measuring results," in *Proc. 9th Mediter. Conf. Embed. Comput. (MECO)*, 2020, pp. 8–11, doi: [10.1109/MECO49872.2020.9134348](https://doi.org/10.1109/MECO49872.2020.9134348).
- [50] S. Moltchanov, I. Levy, Y. Etzion, U. Lerner, D. M. Broday, and B. Fishbain, "On the feasibility of measuring urban air pollution by wireless distributed sensor networks," *Sci. Total Environ.*, vol. 502, pp. 537–547, Jan. 2015, doi: [10.1016/j.scitotenv.2014.09.059](https://doi.org/10.1016/j.scitotenv.2014.09.059).
- [51] P. Kumar, L. Morawska, C. Martani, G. Biskos, M. Neophytou, S. D. Sabatino, M. Bell, L. Norford, and R. Britter, "The rise of low-cost sensing for managing air pollution in cities," *Environ. Int.*, vol. 75, pp. 199–205, Feb. 2015, doi: [10.1016/j.envint.2014.11.019](https://doi.org/10.1016/j.envint.2014.11.019).
- [52] Z. Liu, G. Wang, L. Zhao, and G. Yang, "Multi-points indoor air quality monitoring based on Internet of Things," *IEEE Access*, vol. 9, pp. 70479–70492, 2021, doi: [10.1109/ACCESS.2021.3073681](https://doi.org/10.1109/ACCESS.2021.3073681).
- [53] M. Alvarez-Campana, G. López, E. Vázquez, V. Villagrà, and J. Berrocal, "Smart CEI moncloa: An IoT-based platform for people flow and environmental monitoring on a smart university campus," *Sensors*, vol. 17, no. 12, p. 2856, Dec. 2017, doi: [10.3390/s17122856](https://doi.org/10.3390/s17122856).
- [54] Shanghai SIMCom Wireless. (2018). *Application Note SIM7000 Series*. [Online]. Available: <https://simcom.ee/documents/?dir=SIM7000x>
- [55] O. G. Adewumi, K. Djouani, and A. M. Kurien, "RSSI based indoor and outdoor distance estimation for localization in WSN," *Proc. IEEE Int. Conf. Ind. Technol.*, Feb. 2013, pp. 1534–1539, doi: [10.1109/ICIT.2013.6505900](https://doi.org/10.1109/ICIT.2013.6505900).
- [56] M. Lu-feng, G. Zheng-ge, X. Wei, and L. Zhou, "SAR²: Mitigating the packet loss in wireless sensor networks with self-adaptive repair and regulation," *Comput. Eng. Sci.*, Changsha, China, Tech. Rep., 2010, vol. 32, no. 11, pp. 52–54. [Online]. Available: <http://manu46.magtech.com.cn/ces/EN/article/downloadArticleFile.do?attachType=PDF&id=12235>
- [57] R. Shazwani Rosli, M. Hadi Habaebi, and M. R. Islam, "Analysis of different digital filters for received signal strength indicator," *Bull. Electr. Eng. Informat.*, vol. 8, no. 3, pp. 970–977, Feb. 2019, doi: [10.11591/eei.v8i3.1508](https://doi.org/10.11591/eei.v8i3.1508).
- [58] E. J. Ofure, O. O. David, A. M. Oludare, and A. A. Musa, "Impact of some atmospheric parameters on GSM signals," in *Proc. 13th Int. Conf. Electron. Comput. Comput. (ICECCO)*, Jan. 2018, pp. 1–7, doi: [10.1109/ICECCO.2017.8333335](https://doi.org/10.1109/ICECCO.2017.8333335).
- [59] Z. Mihajlovic, V. Milosavljevic, V. Rajs, and M. Zivanov, "Application of GPRS modules in data acquisition and control of devices for air quality monitoring," in *Proc. 20th Telecommun. Forum (TELFOR)*, Nov. 2012, pp. 1020–1023.
- [60] US EPA. (2018). *Technical Assistance Document for the Reporting of Daily Air Quality—The Air Quality Index (AQI)*. [Online]. Available: <https://airnowtest.epa.gov/sites/default/files/2018-05/aqi-technical-assistance-document-may2016.pdf>
- [61] S. Archasantisuk, T. Aoyagi, M. Kim, and J. Takada, "Temporal correlation model-based transmission power control in wireless body area network," *IET Wireless Sensor Syst.*, vol. 8, no. 5, pp. 191–199, Oct. 2018, doi: [10.1049/iet-wss.2016.0109](https://doi.org/10.1049/iet-wss.2016.0109).
- [62] H. Wang, F. Zhang, and W. Zhang, "Human detection through RSSI processing with packet dropout in wireless sensor network," *J. Sensors*, vol. 2020, pp. 1–9, Sep. 2020, doi: [10.1155/2020/4758103](https://doi.org/10.1155/2020/4758103).
- [63] J. Gutierrez, J. F. Villa-Medina, A. Nieto-Garibay, and M. A. Porta-Gandara, "Automated irrigation system using a wireless sensor network and GPRS module," *IEEE Trans. Instrum. Meas.*, vol. 63, no. 1, pp. 166–176, Jan. 2014, doi: [10.1109/TIM.2013.2276487](https://doi.org/10.1109/TIM.2013.2276487).
- [64] A. Lo Schiavo, "Fully autonomous wireless sensor network for freight wagon monitoring," *IEEE Sensors J.*, vol. 16, no. 24, pp. 9053–9063, Dec. 2016, doi: [10.1109/JSEN.2016.2620149](https://doi.org/10.1109/JSEN.2016.2620149).
- [65] H. Wang, L. Dong, W. Wei, W.-S. Zhao, K. Xu, and G. Wang, "The WSN monitoring system for large outdoor advertising boards based on ZigBee and MEMS sensor," *IEEE Sensors J.*, vol. 18, no. 3, pp. 1314–1323, Feb. 2018, doi: [10.1109/JSEN.2017.2770324](https://doi.org/10.1109/JSEN.2017.2770324).



RADY PURBAKAWACA (Graduate Student Member, IEEE) received the B.Sc. degree (Hons.) from the Department of Physics, IPB University, Indonesia, in 2013, and the M.Sc. degree from the Department of Civil and Environmental Engineering, IPB University, in 2015, where he is currently pursuing the Ph.D. degree with the Department of Mechanical and Biosystem Engineering. His research interests include the Internet of Things, machine-to-machine networks, big data, environ-

mental monitoring, embedded systems, and instrumentation and control systems.



ARIEF SABDO YUWONO received the B.S. degree in agricultural engineering from Bogor Agricultural University, Indonesia, in 1989, the M.Sc. degree in environmental sanitation from Universiteit Gent, Belgium, in 1996, and the Ph.D. degree in bioenvironmental engineering from Universitaet Bonn, Germany, in 2003. He is currently a Professor in civil and environmental engineering at the Faculty of Agricultural Engineering and Technology, IPB University. He was an Air Quality and Noise Expert, an Air Emission Expert, and an Environmental and Agricultural Specialist. His research interests include environmental monitoring, environmental instrumentation, and water and air pollution quality controls.



ests include automation and robotics in agriculture.

I. DEWA MADE SUBRATA received the bachelor's degree from Bogor Agricultural University, in 1986, the M.S. degree from Shimane University, Japan, in 1995, and the Ph.D. degree from the United Graduate School of Agricultural Sciences, Tottori University, Japan, in 1998. He is currently an Associate Professor with the Department of Mechanical and Biosystem Engineering, Faculty of Agricultural Engineering and Technology, IPB University, Bogor, Indonesia. His research interests include automation and robotics in agriculture.



monitoring, instrumentation, and control systems.

SUPANDI received the bachelor's degree in metallurgical engineering from the Industrial Military Academy, in 1982, and the master's degree from Satyagama University, in 1995. He is currently a Co-Researcher in environmental engineering from the Unilab Perdana (Environment and Calibration Laboratory). He is also the Chairman of the Indonesian Society for Standardization and the Founder of the Indonesian ISO Expert Association. His research interests include environmental



research interests include the theory and modeling of photonic crystal-based sensors. He is also a member of the Indonesian Center for Theoretical and Mathematical Physics (ICTMP), the Indonesian Optical Society (InOS), and *Optica* (formerly OSA).

HUSIN ALATAS received the B.S., M.Sc., and Ph.D. degrees from the Bandung Institute of Technology, Indonesia, in 1995, 1998, and 2005, respectively. He is currently a Professor with the Physics Department, Faculty of Mathematics and Natural Sciences, IPB University, Bogor, Indonesia. He is also the Head of the Theoretical Physics Division, IPB University, where he is also the Executive Secretary of the Center for Transdisciplinary and Sustainability Sciences (CTSS). His

...